Cement and Concrete Composites 143 (2023) 105259

Contents lists available at ScienceDirect

Cement and Concrete Composites

journal homepage: www.elsevier.com/locate/cemconcomp

Assessing the potential application of bacteria-based self-healing cementitious materials for enhancing durability of wastewater treatment infrastructure

Manpreet Bagga [a,1], Ismael Justo-Reinoso [b,1], Charlotte Hamley-Bennett [c], George Merces [d], Saimir Luli [e], Ange Therese Akono [f], Enrico Masoero [g], Kevin Paine [b], Susanne Gebhard [c,h], Irina D. Ofiţeru [a,*]

[a] School of Engineering, Newcastle University, Newcastle Upon Tyne, UK
[b] Centre for Climate Adaptation and Environment Research, University of Bath, Bath, UK
[c] Department of Life Sciences, University of Bath, Bath, UK
[d] Bio-Imaging Unit, Medical School, Newcastle University, Newcastle Upon Tyne, UK
[e] Preclinical In Vivo Imaging, Translational and Clinical Research Institute, Newcastle University, Newcastle Upon Tyne, UK
[f] Department of Civil and Environmental Engineering, Northwestern University, USA
[g] School of Engineering, Cardiff University, Cardiff, UK
[h] Institute of Molecular Physiology, Johannes Gutenberg-Universität Mainz, Mainz, Germany

ARTICLE INFO

Keywords:
Self-healing
MICP
Field application
Wastewater
Sustainability

ABSTRACT

Wastewater treatment plants (WWTPs) around the world are mainly built using concrete. The continuous exposure to wastewater affects the durability of concrete structures and requires costly maintenance or replacement. Concrete production and repair represents ~8% of the global anthropogenic CO_2 emissions due to the use of cement, thus contributing to climate change. Developing a more sustainable cementitious material is therefore required for this vital health infrastructure. In this study, the feasibility of using bacteria-based self-healing (BBSH) cementitious materials for WWTPs is assessed by exposing BBSH mortar prisms to a continuous municipal wastewater flow and comparing their self-healing capacity to equivalent mortar prisms exposed to tap water. Microscopy imaging, water-flow tests and micro-CT analyses were performed to evaluate the self-healing efficiency of the mortar prisms, while SEM-EDX and Raman spectroscopy were used to characterise the healing products. Our work represents the first systematic study of the healing potential of BBSH in mortar exposed to wastewater. The results indicate that the purposely added bacteria are able to induce calcium carbonate precipitation when exposed to wastewater conditions. Moreover, if additional sources of calcium and carbon are embedded within the cement matrix, the rich bacterial community inherently present in the wastewater is capable of inducing calcium carbonate precipitation, even if no bacteria are purposely added to the mortar. The results of this study offer promising avenues for the construction of more sustainable wastewater infrastructure, with the potential of significantly reducing costs and simplifying the production process of BBSH concretes for this specific application.

1. Introduction

Wastewater treatment plants (WWTPs) are designed to remove pollutants and pathogenic organisms from water that has been previously used and contaminated and that needs to be discharged within specific water quality limits [1,2]. The collection and treatment of wastewater have required huge investments in the past decades across Europe, where more than 18,000 WWTPs exist [3]. In this context, the Organisation for Economic Co-operation and Development (OECD) estimates that €253 billion will need to be spent between 2020 and 2030 by EU countries and the United Kingdom to reach and ensure full compliance with the Urban WasteWater Treatment Directive

* Corresponding author.
E-mail address: dana.ofiteru@ncl.ac.uk (I.D. Ofiţeru).
[1] These authors contributed equally.

https://doi.org/10.1016/j.cemconcomp.2023.105259
Received 19 April 2023; Received in revised form 25 July 2023; Accepted 16 August 2023
Available online 19 August 2023

(UWWTD-91/271/EEC) [4]. As human society heavily relies upon this crucial sanitary infrastructure to reduce diseases and prevent biodiversity loss in the areas surrounding the discharge of the treated effluent, any interruption in their operation can have catastrophic results. Nevertheless, WWTPs construction and operation have also an extensive cost and environmental impact related to energy and materials consumption, aeration required during treatment process, direct greenhouse gas emissions, repair and other operational costs [5,6]. Therefore, it is crucial to use durable and low-maintenance materials for their construction as this will reduce their negative environmental impact [7]. The durability of WWTPs is a major concern of governments worldwide as it is directly related to the risk of having significant social, economic and environmental impacts. As a result, nowadays, most WWTPs worldwide are built using reinforced concrete [8], as very few materials can withstand the aggressive nature of wastewater. However, although concrete is considered durable when exposed to common environmental conditions, it is affected by the corrosive nature of wastewater and rapidly deteriorates in WWTPs [9]. Acid and sulphate attack, along with carbonation, erosion, cavitation and biogenic degradation, are major threats to the durability of WWTPs [8]. All of these can lead to expansion, cracking, lack of strength and deterioration of concrete walls [10]. With time, these cracks allow harmful agents to migrate deep inside the concrete structure, triggering the corrosion process of reinforcement steel, which in the long run, causes the deterioration and subsequent collapse of WWTPs. Therefore, different self-healing technologies have been developed to help cementitious materials re-close appearing cracks and, in this way, increase their durability [11,12].

Among these technologies, bacteria-based self-healing (BBSH) has stood out in the past decade for its great potential to achieve more sustainable concretes by taking advantage of the inherent capability of some specific bacteria to induce calcium carbonate precipitation [13]. BBSH can increase the durability and life span of concrete structures thus reducing environmental impact caused by maintenance and repair of the cracks developed over time. In this context, extensive research has been done to develop BBSH concretes (BBSHCs) using microbial induced calcite precipitation (MICP), as reflected in the number of papers published in journals since 2009 [14,15]. MICP relies on the negatively charged surface of bacteria cells to draw calcium ions present in the environment to accumulate around bacteria, where they react with carbonate ions and precipitate as calcium carbonate [16]. Different MICP pathways have been considered to achieve self-healing cementitious materials. Among these, the use of both ureolytic and non-ureolytic bacteria have been considered [15,17]. However, using ureolytic bacteria has a major drawback in producing nitrogen oxide emissions which causes environmental and health concerns [18,19]. In this regard, the use of non-ureolytic bacteria represents a potentially more sustainable alternative that could find important applications in wastewater infrastructure [17].

In this study, we tested the healing potential of a selected environmental bacterial strain capable of precipitating calcium carbonate via a non-ureolytic process. The bacterial spores, encapsulated into aerated concrete granules (ACGs), were used to fabricate mortar prisms, which were cracked after 28 days of curing submerged in water. Then, two sets of equivalent mortar prisms were exposed independently for 56 days to two healing conditions (i) tap water (laboratory) and (ii) wastewater (municipal wastewater treatment pilot plant) to test the feasibility of using BBSH cementitious materials in wastewater infrastructure. The self-healing efficiency of the mortar prisms was evaluated using microscopy imaging, water-flow tests and micro-CT analyses, while the healing products were characterised using SEM-EDX and Raman spectroscopy.

2. Materials and methods

2.1. Bacterial species and spore production

A non-ureolytic spore-forming soil bacterium (CGN12) was selected from the library reported in Ref. [20] and stored in glycerol (50% wt./vol) at −80 °C [20]. The spores were produced in 2L and 5L jacketed bioreactors (Applikon ez2-Controls, Getinge, UK) by growing the CGN12 cells in Difco sporulation medium for 6 days [21]. The initial pH of the medium was set to 7.6 using 1 M NaOH solution, and 100 μl/L of Antifoam B Emulsion (aqueous-silicone) was added in the bioreactors to prevent excessive foaming. The reactors were inoculated when the probes for temperature and dissolved oxygen displayed stable values. The inoculum for spore production was obtained from overnight CGN12 cell cultures in lysogeny broth (LB) adjusted to pH 8.2 with 20 mM Tris/HCl. Reactors were maintained at a constant 30 °C temperature and 1 vvm aeration with the impeller set at 150 rpm. The spores pellet was harvested by centrifuging at 3041×*g* for 10 min, washed following the method described in Ref. [21], and then frozen at −80 °C. The pellet was then freeze-dried under vacuum for 24 h using a ModulyoD freeze dryer (Thermo Electron Corporation, USA). Spore viable count was determined by suspending 1 mg of the dried spore powder in 1 mL LB medium, followed by serial dilution and plating on LB agar. Unless otherwise specified, all the chemicals used in this study were obtained from Merck (UK).

2.2. Growth media (GM) added in the mortar prisms

Two sets of mortar prisms were produced in this study: Set I and Set II. The growth media for Set I (GM_I) contained calcium nitrate tetrahydrate (5% wt./wt. cement) and yeast extract (1% wt./wt. cement), while for Set II, the growth media (GM_II) consisted of calcium nitrate tetrahydrate (5% wt./wt. cement), sodium acetate anhydrous (3.5% wt./wt. cement) and yeast extract (0.2% wt./wt. cement).

2.3. Encapsulation with aerated concrete granules (ACGs)

Aerated concrete granules (ACGs) were used as the carrier for bacterial spores. ACGs were supplied by Cellumat SA (Belgium) and sieved to obtain a particle size gradation between 1 and 4 mm. ACGs had a loose dry bulk density and absorption capacity of 354 kg/m^3 and 120%, respectively [22,23]. ACGS were utilised in selected mortar mixes with or without embedded bacterial spores. For ACGs containing bacterial spores, a bacterial spore suspension composed of distilled water (4.3 mL) and CGN12 spores (1.0×10^{10} colony-forming units (CFU)) was incorporated into 3.54 g of ACG particles by using a vacuum saturation technique, as fully described in Ref. [22]. After the encapsulation process, the ACGs were kept for 24 h under ambient laboratory conditions (20 °C, 50% relative humidity (RH)) to obtain a dry surface. Next, dry ACG particles, with and without bacterial spores, were coated with polyvinyl acetate (PVA; 50% (wt./wt.)) supplied by Henkel Ltd (UK). Both types of PVA-coated ACGs were stored separately in Ziploc® plastic bags on lab benchtop until further use.

2.4. Preparation of mortar prisms

The experimental programme was separated into two main sets consisting of mortar prism specimens (40 mm × 40 mm x 65 mm). Mortar prisms in Set I were prepared using calcium nitrate and yeast extract as the calcium and carbon sources, respectively. Mortar prisms in Set II were produced using sodium acetate as the carbon source, a trace of yeast extract as a source of essential amino acids, and again, calcium nitrate as the calcium source. All mortar prisms for Set I and Set II were cast and cured for 28 days submerged in tap water. Half of each Set was then used to evaluate the self-healing capacity when exposed to municipal wastewater, while the other half was exposed to tap water

under ambient laboratory conditions. The abbreviation syntax for the mortar formulations was as follows: labelled first by the Set (SI for 'Set I' and SII for 'Set II'); followed by the base mortar formulation (R for plain mortar, R + GM_I for plain mortar with GM_I, R + C for plain mortar with direct addition of calcium nitrate, R + YA for plain mortar with direct addition of sodium acetate and R + GM_II for plain mortar with direct addition of GM_II); lastly, the bacterial spores content: ACG-Ø (ACG without spores) and ACG-S (ACG with spores). All the cement mortar formulations were prepared in sextuplets using Portland limestone cement (CEM II/A-L 32.5R) and standard sand conforming to BS EN 197-1 and BS EN 196-1, respectively. All mortar formulations were standardised to a water/cement (w/c) ratio of 0.5 using local tap water. Details on the materials used, the mortar formulations and the notation used throughout this study are given in Table 1.

The procedure for mixing the materials was adapted from BS EN 196-1 as follows. First, if the mortar formulation included calcium nitrate, sodium acetate or yeast extract, these were added to the total amount of mixing water and manually mixed for 30 s. Next, cement was added to the total amount of water and manually mixed for an additional 30 s. After the initial manual mixing (60 s), further mixing was carried out using an automatic mortar mixer (Automix Controls, UK) for 240 s. In the case of formulations containing ACG-Ø or ACG-S, the ACG particles were dry mixed with the total amount of standard sand before adding the sand and the ACG particles to the automatic mixer.

Only the bottom layer (20 mm) of each prism was self-healing mortar (as per the proportions in Table 1), while the top layer (top 20 mm) contained plain mortar in all cases. The bottom layer was cast first, and after approximately 100 min, the top layer was then cast on top. In a similar way, plain mortar prisms (i.e., SI_R and SII_R) were also cast in two layers, each of them of plain mortar. Mortar prisms were kept at ambient laboratory conditions until they were demoulded. Given the known property of yeast extract to delay the setting time of cement mortar formulations [24], a consistent demoulding time of 48 h was chosen to ensure uniformity and prevent any potential damage to the specimens from premature demoulding. This demoulding timeframe has been previously used by the authors in similar studies involving yeast extract in cement mortar preparation [20,25]. After demoulding and until the day before cracking, all mortar prisms were cured submerged in local tap water at 20 °C ± 3 °C. Separate 10L plastic containers were used for the six specimens of each formulation to avoid any possible cross-contamination.

2.5. Cracking of mortar prisms

After the curing period, all mortar prisms were dried at ambient laboratory conditions for 24 h. Following this, a notch of 1.5 mm depth was sawn at the centre of each mortar prism to induce crack formation. Then, carbon fibre-reinforced polymer (CFRP) strips were affixed to the top third of the mortar prisms using an EL2 epoxy laminating resin (Easy Composites, Stoke-on-Trent, UK) to guarantee the integrity of the samples after cracking (See Appendix A). Mortar prisms were cracked by three-point bending using a 100 kN Dartec-Instron hydraulic loading frame. After the crack was formed and while maintaining the load, two 0.5 mm thick plastic spacers were placed at both ends of the formed crack, as fully described in Ref. [25]. Three selected crack locations (separated 10 mm from each other and the borders of the specimen) were marked with a permanent marker to enable monitoring of the crack at the same site. Immediately after cracking, the cracks were inspected using an optical microscope before placing the mortar prisms under healing conditions.

2.6. Healing conditions for mortar prisms

2.6.1. Tap water healing

Mortar prisms were placed in independent containers with tap water and kept open to the atmosphere. The side of the mortar prism containing the crack was facing upwards, while the water level was maintained constant at 10 mm below the top of the specimen (i.e., the crack surface is not under water). The mortar prisms were kept at ambient laboratory temperature (20 °C ± 3 °C) for 56 days and periodically inspected. Before each periodic visual observation of the cracks, mortar prisms were removed from the water and left to dry for 2 h to obtain an unwetted crack surface. This pre-drying step was necessary to avoid reflection of microscope lights by wet surfaces [26,27].

2.6.2. Wastewater healing

A duplicate set of mortar prisms (nominally identical to the ones kept in tap water) were tested at the BEWISe pilot plant facility. The pilot plant is located inside the Northumbrian Water Ltd WWTP at Birtley (UK) which treats municipal wastewater (30,000 population equivalent). The mortar prisms were placed in a hopper within a tray of 30 mm height (Fig. 1), with the cracked side facing upwards. The hopper received a continuous flow of untreated municipal wastewater, identical to the one in the WWTP. The wastewater level was maintained 10 mm below the top of the mortar prisms, in a similar way to the tap-water-exposed mortar prisms. The mortar prisms were randomly distributed within the tray and their position was changed every week, to avoid any preferential healing due to the proximity of the prisms to the wastewater inlet.

The inlet pipe was fitted with dissolved oxygen (DO), pH and temperature probes, and these parameters were measured continuously during the period of 56 days of the experiment. Three samples of wastewater were collected on days 0, 28, and 56, respectively, to measure the concentration of urea, ammonium ions and cations present in the water. Urea and ammonium ions were measured using the standard urea assay kit (Sigma-Aldrich, UK) and Macherey Nagel Quantofix Ammonium Test Kit (Fisher Scientific, UK), respectively. The concentration of different cations was measured using an Inductively Coupled Plasma-Optical Emissions Spectrometer ICP-OES 5800 (Agilent Technologies, US). One wastewater sample directly from the inlet pipe and one from the more stagnant layer accumulated in the tray were also collected during the healing experiment and sequenced to evaluate the

Table 1
Mortar proportions for producing the bottom layer of all mortar formulations used in this study (six mortar prisms per formulation (40 mm × 40 mm x 65 mm)).

Mortar formulation	Cement (g)	Water (mL)	Standard sand (g)	Calcium nitrate (g)	Yeast extract (g)	Sodium acetate (g)	CGN12 spores (CFU)	ACG-Ø (g)	ACG-S (g)
SI_R	184	92	552	0	0	0	0	0	0
SI_R + GM_I_ACG-Ø	184	92	525.4	9.2	1.8	0	0	5.3	0
SI_R + GM_I_ACG-S	184	92	525.4	9.2	1.8	0	1.0×10^{10}	0	5.3
SII_R	184	92	552	0	0	0	0	0	0
SII_R + C_ ACG-Ø	184	92	532.2	9.2	0	0	0	0	0
SII_R + YA_ ACG-Ø	184	92	534.6	0	0.4	6.4	0	0	0
SII_R + GM_II_ACG-Ø	184	92	525.4	9.2	0.4	6.4	0	5.3	0
SII_R + GM_II_ACG-S	184	92	525.4	9.2	0.4	6.4	1.0×10^{10}	0	5.3

Fig. 1. Mortar prisms placement in the BEWISe pilot treatment plant. The inner tray of the hopper was subject to a continuous flow of municipal wastewater from the overhead tap. A small pipe extension was attached to the tap to prevent splashing. The inner tray, in which the samples were placed, had a height of 30 mm, allowing the top 10 mm of the mortar prisms to be exposed to air.

typical composition of the metagenome. The sequence was performed by Novogene, UK (Shotgun Metagenomics (WOBI) Sequencing, NovaSeq PE150, 10 Gb raw data per sample).

2.7. Investigation of self-healing efficiency

2.7.1. Microscope imaging and area quantification of the cracks

Visualisation of crack healing was periodically carried out for tap water and wastewater-exposed mortar prisms using a digital microscope VHX-6000 (Keyence, Japan) and a portable microscope (Celestron, USA), respectively. A verification process was conducted at the beginning of the study to ensure consistent accuracy between both microscopes (See Appendix A). Images were taken immediately after cracking (0 days) and after 7, 14, 21, 28 and 56 days of healing. The complete crack images of the wastewater-exposed mortar prisms were created by overlapping individual images using an open-source vector editing software (Inkscape 1.0.1). For the tap-water-exposed specimens, a seamless complete crack image was directly obtained using the automated image stitching option of the digital microscope. Then, image binarization was conducted to quantify the crack area reduction over time using the open-source image processing software ImageJ [28]. First, the original image was converted to an 8-bit image, and a black threshold level of 110 was applied. Similar threshold values have been used in other studies where crack healing has also been investigated [25, 29–32]. Then, the number of crack area pixels or each mortar prism before and after healing was counted. The crack-area healing ratio was measured as the decrease in the fraction area of black pixels corresponding to the cracks in the images taken immediately after cracking and after 56 days of healing. The crack-area healing ratio percentage (CAH%) was calculated according to **equation (1)**:

$$\mathrm{CAH\%} = \frac{A_i - A_f}{A_i} \cdot 100 \tag{1}$$

where A_i and A_f are the initial and final area (respectively) of the complete crack per individual mortar prism.

2.7.2. Water tightness recovery

The ability of the cracks to successfully achieve water tightness was quantified with a water-flow test, based on RILEM test Method 11.4 [33]. This method is a well-established and proven technique for evaluating the recovery of water-tightness in self-healing cementitious materials. Additionally, it offers the advantage of being relatively fast compared to other commonly used test methods. This speed was particularly advantageous in this study for testing the 'in-situ' mortar prisms permanently located at the BEWISe pilot plant facility. Furthermore, the triangular shape of the crack, as utilised in this method, is considered to better represent real-life cracks compared to other techniques that require a complete through-depth crack [34]

The water-flow tests were carried out immediately after cracking and after 28 and 56 days of healing. The water-flow coefficient (k) was calculated according to **equation (2)** [25,32] The authors utilised an apparatus similar to that used in previous studies [22]. The equation for obtaining k is as follows:

$$k = \frac{a \cdot L}{A \cdot t} \ln\left[\frac{h1}{h2}\right] \tag{2}$$

where k is the water-flow coefficient (cm/s); a is the cross-sectional area of the cylinder (1.13 cm^2); L is the thickness of the mortar prism (4 cm); A is the contact area of the base of the apparatus with the mortar prism (9.6 cm^2); t is the time required for the water level to move from h_1 (initial water head, 12.4 cm) to h_2 (final water head (cm)). The percentage of crack healing (CH%) ratios was calculated according to **equation (3)**:

$$\mathrm{CH\%} = \frac{k_0 - k_t}{k_0} \cdot 100 \tag{3}$$

where k_0 is the initial water-flow coefficient, and k_t is the water-flow coefficient at healing time t.

2.7.3. X-ray micro-CT scanning

The overall healing of the cracks within the mortar prisms exposed to wastewater was quantified by comparing X-ray micro-computed tomography (micro-CT) images taken at Day 0 (post-cracking) and Day 56 (after the healing period). One mortar prism of each set of triplicate samples of Set II was left to air dry at room temperature and wrapped in cling film before the scan to prevent cross-contamination within the instrument. The mortar prisms were analysed using the Skyscan 1176 (Bruker, USA) at an isotropic resolution of 35 μm using a source voltage of 90 kV, 278 μA current, and 0.1 mm copper filter. Mortar prisms were scanned at 360° with a rotation step of 0.5° with 2 averages per frame with an exposure time of 105 ms. GPUReconServer and NRecon Reconstruction 64-bit software (Bruker, USA) were used to reconstruct raw projections data. CTvox (Version 3.3.0, Bruker) was used for 3D volume rendering and data visualisation.

2.7.3.1. Image cropping and re-slicing. Reconstructed image stacks were then rotated using open-source software Fiji [35] to ensure that the outer edges of the mortar prisms lined up with the image X and Y axes. The mortar prism area was manually selected within Fiji software using the box selection tool, with the whole stack assessed to ensure the mortar prism remained within the confines of the box throughout the stack. The stack was then re-sliced from the top using the "Reslice" function to create a new stack from the perpendicular angle of the mortar prism, allowing visualisation of the fully induced crack throughout the mortar prism width.

2.7.3.2. Manual gap distance measurement. The opening of the crack, indicated by the indentation along the mortar prism at the point of crack induction, was assessed manually. Reference points were determined between the pre-treatment and post-treatment scans of the mortar prisms, allowing direct before/after comparison of the gap distance. The distance was measured between the walls of the crack at this opening, immediately after the semi-circular indentation, by drawing a line using the Fiji line tool, measuring the length of the line in pixels between the two walls. The gap distance was measured at 11 matched points along the opening of the crack for each of the paired datasets, 100 slices apart,

spanning almost the entirety of the crack opening.

2.7.3.3. Manual crack intensity distance measurement. Reference points were determined between the Day 0 and Day 56 scans of the mortar prisms, allowing a direct before and after healing comparison. At each of the 11 reference points (100 slices apart), the crack was traced using the Fiji segmented line tool. The intensity along the line, starting at the crack opening, was measured within Fiji for each of the traced cracks. The intensity was normalised by subtracting the mean background intensity from within the semi-circular indentation, measured separately for each mortar prism at each time point. The output data was collated in RStudio, with mean data generated using the distance from the start of the crack tracing to group data from the same dataset. Pixel intensity measurements for each pixel along the crack length were averaged for each group and plotted using the Geom_Smooth function within RStudio (using Method = loess and formula y ~ x), with confidence intervals of 95% shown on either side of the smoothed line of fit.

2.8. Microstructural analyses

2.8.1. SEM-EDX

The SEM-EDX analyses were carried out for one mortar prism from each set of samples, from both tap-water and wastewater-exposed mortar prisms. Scanning was performed at multiple points, as shown in Fig. 2, using a JSM-IT510 microscope (Jeol, Japan) fitted with a Ultim Max Symmetry EDX detector (Oxford Instruments, UK). After 56 days of healing and once the mortar prisms were air-dried, they were attached to the aluminium holder on the microscope using a double-sided carbon sticky tape. A sticky aluminium tape was used to ground the samples, which helped dissipate the electrons from the surface of the prisms. The acceleration voltage and current were set for 20 kV and 30 μA, respectively.

2.8.2. Raman spectroscopy

The chemical structure of the healing product was analysed using LabRam HR800 Raman spectrometer (HORIBA Jobin Yvon, UK). An argon laser of 514 nm wavelength, with 1800 grating and 100% filter with 20 s acquisition time and 3 averages, was used to acquire the spectra. All the Raman spectra were taken at the centre of the cracks due to physical limitations with the objective lens used (×10). The data were analysed to reduce the background noise and compare different samples using the open-source optical spectroscopy software Spectragryph 1.2.

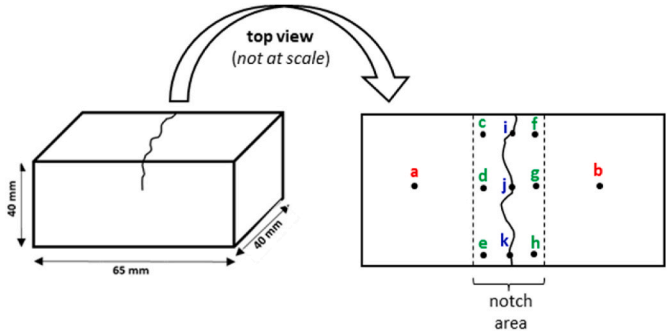

Fig. 2. Schematic of the SEM-EDX analysis. Images were taken at three points on the crack (i, j and k) to visualise the healing product, six points on both sides of the crack (c, d, and e on the left-hand side; and f, g and h on the right-hand side) and two points in the centre of the mortar prisms on both the side of the crack (a and b) to estimate the amount of calcium available in the mortar prism after 56 days of healing in tap water or wastewater conditions.

3. Results

3.1. Wastewater and tap water analyses

The average and standard deviation of DO, pH and temperature for wastewater measured continuously with the online sensors over the period of healing (56 days) for the Set II samples were 0.22 ± 0.098 mg/L, 6.88 ± 0.26 and 17.86 ± 0.78 °C respectively. The wastewater composition for calcium ions, potassium, magnesium, and silicon was on average of 49.92 ± 3.04, 18.48 ± 0.45, 7.86 ± 0.36 and 3.96 ± 0.47 mg/L, respectively. The concentration of urea was between 32.58 and 91.4 mg/L. The Quantofix test strip indicated the colour corresponding to 50 mg/L concentration of ammonium ion. The pH range and the mean calcium ion concentration of the tap water (as reported by the water supplier, Wessex Water Ltd) was between 7.30 and 7.70 and 110.17 mg/L, respectively, and the samples were kept at room temperature. The bacterial metagenome in both wastewater samples analysed (collected from the tap and from the inner tray, respectively) showed a great diversity and were dominated by phylum Proteobacteria, with the Terrabacteria Group, which include the Bacilli commonly used in self-healing concrete applications as well as CNG12, forming the second largest group (see Appendix B for the Krona metagenomic visualisation [36]).

3.2. Self-healing efficiency

The evaluation of BBSH efficiency of cementitious materials is typically conducted under controlled laboratory conditions and using clean tap water during the healing process. It is expected that real environmental conditions, where the specific bacteria deliberately added to the self-healing concrete will have to interact and likely compete with naturally present bacteria, could have a significant impact on the self-healing efficiency. In this study, two sets of mortar prisms with different organic carbon provisions (i.e., yeast extract or sodium acetate for Set I and Set II, respectively) were cracked and allowed to heal for 56 days. Half the mortar prisms of each set were exposed to controlled laboratory conditions (tap water), while the remaining mortar prisms were exposed to a realistic application setting, i.e., a continuous wastewater flow at a wastewater pilot plant. Quantification of the reduction in crack area and water-flow tests were conducted on all the mortar prisms to evaluate their self-healing efficiency when exposed to the two different healing regimes. Moreover, micro-CT scans were obtained from a representative mortar prism of each formulation and analysed to evaluate crack closure over time and healing product formation inside the crack.

3.2.1. Crack-area quantification

In the first step of the experiments, a previously proven successful BBSH mortar formulation [20,22,25], where yeast extract was used as the only purposely added carbon source (Set I), was exposed to the two healing conditions (i.e., tap water and wastewater). In Fig. 3, the crack-area healing percentage (CAH%) results for the mortar prisms of Set I when exposed to the two different healing regimes are presented. No significant healing was observed in any of the mortar prisms of the plain mortar mix (i.e., SI_R). In contrast, considerable healing was observed for the mortar mixes containing yeast extract and calcium nitrate (i.e., SI_R_GM_I_ACG-Ø and SI_R_GM_I_ACG-S), where mortar prisms exposed to wastewater presented a significantly higher degree of healing (up to 52% higher) when compared to prisms exposed to tap water. The complete crack images for all the different mortar prisms of Set I, before and after the binarization process, are presented in Appendix C.

From the CAH% results obtained from Set I mortar prisms, it is not possible to clearly identify the individual contribution of each of the additions (i.e., calcium or yeast extract) to the healing efficiency. Therefore, a second set of mortar prisms (Set II), where two additional

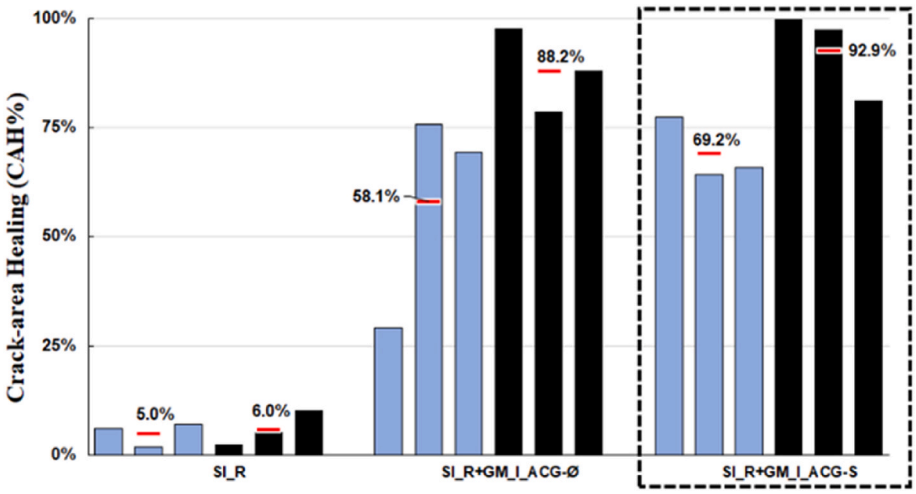

Fig. 3. Crack-area healing percentage (CAH%) for Set I mortar specimens after 56 days of healing. Bars represent the CAH% obtained as a function of crack-area reduction of the individual mortar specimens exposed during the healing period to: (■) tap water and (■) wastewater. The dotted box shows the mortar prisms containing bacterial spores encapsulated into aerated concrete granules (ACGs). Horizontal bars show the average values for each triplet of mortar prisms.

mortar mixes, containing either the carbon or calcium sources separately, were cast and exposed to the two different healing regimes. However, for Set II, sodium acetate was used as the principal organic carbon source and yeast extract was present only as a trace nutrient. The substitution of the organic carbon source was based not only on reducing scaling-up production costs of this technology, as yeast extract is at least twice more expensive than sodium acetate, but also to ensure a more standard admixture as for sodium acetate the exact chemical composition is well known while that of the yeast extract is highly variable [37]. Additionally, the inclusion of yeast extract can result in longer setting times which could lead to increased construction costs [37–39]. For Set II mortar prisms, Figs. 4 and 5 show the complete crack images before and after the binarization process, post-cracking (Day 0) and after the healing period (Day 56), for a representative mortar prism of each mix when these were healed in tap water or wastewater, respectively.

By comparing the initial crack area with the area remaining after the healing process, the healing of the cracks can be evaluated. Therefore, using the binarized images of the complete cracks taken immediately after cracking (Day 0) and at the end of the healing period (Day 56), the reduction of the crack area over time was quantified. In Fig. 6, the crack-area healing percentages (CAH%) obtained from the crack-area quantification for the Set II mortar prisms exposed to tap water and wastewater are presented.

It is important to note that only one plain mortar prism (i.e., SII_R) was exposed to tap water, as the other two mortar prisms of the triplet were damaged during the cracking process. In general, mortar prisms not containing direct addition of calcium nitrate (i.e., SII_R and SII_R + YA_ACG-Ø) presented low healing efficiency (between 1.5% and 26.3%) for both tap water and wastewater conditions. Mortar prisms exposed to wastewater had more inconsistent healing values when compared to mortar prisms exposed to tap water. This likely resulted from the significant amount of suspended solids attached to the healed crack at the end of the healing period (i.e., 56 days), as can be seen in Fig. 5. Even though the healed cracks were gently rinsed with tap water to remove any accumulated solids before taking images of the healed crack, not all the solids could be removed. Therefore, in wastewater conditions, the sedimentation and accumulation of suspended solids and consequent cleaning required to remove them might have likely affected the correct visual appreciation of the healed crack on the binarized image.

3.2.2. Water-flow tests

The evaluation of the self-healing performance by quantifying the reduction in the crack area over time relies on a visual evaluation which needs to be complemented with additional tests to fully assess the recovery of the original water-tightness capacity of these mortar prisms. For this purpose, water-flow tests were conducted for both healing conditions (i.e., tap water and wastewater) immediately after forming the crack (Day 0) and after 28 and 56 days of healing to confirm the sealing efficiency of the healed cracks. Water-flow tests were not performed at 7, 14 and 21 days to avoid the risk of removing newly formed healing products, as has been suggested in similar studies [25,27].

The percentage of healing as a function of the water-tightness recovery after 28 and 56 days of healing for each of the mortar prisms exposed to tap water and wastewater healing conditions is shown in Fig. 7. As expected, the tap-water-exposed mortar prisms presented a reduction in the water flow consistent with the crack-area reductions observed in Fig. 6. In contrast, the water-flow results for the wastewater-exposed mortar prisms were not consistent with the crack-area reductions observed for these mortar prisms. These discrepancies can be attributed to the amount of suspended solids in the wastewater influent that were deposited over time within the crack. It is hypothesised that these deposited solids have likely clogged the interior of the crack, significantly reducing the water flow and resulting in a confounding factor that makes it difficult to assess the healing efficiency of the wastewater-exposed specimens using water-flow tests.

3.3. Micro-CT imaging and crack closing

Micro-CT scanning was done on one mortar prism from Set II samples placed in wastewater to quantify the precipitation within the depth of the crack and analyse the crack closure for wastewater samples. The crack width was measured using ImageJ on reconstructed micro-CT images (see Appendix D). The measurement was made on 11 different points, 100 pixels apart, on the same slice of image for Day 0 and Day 56 scans. The distribution of the 11 points (as dots) is shown in the form of a violin plot and its probability density, see Fig. 8 (with red for the crack width on Day 0 and blue for the crack width on Day 56). In this representation, a better healing is considered if the points between Day 0 and Day 56 are further apart for the same sample. For most of the mortar prisms, the cumulative crack width was reduced in the two months they were exposed to wastewater. SII_R + C_ ACG-Ø shows the maximum reduction in crack width, followed by SII_R + GM_II_ACG-S. For SII_R + YA_ACG-Ø uneven amount of precipitate formation can be seen as all the points were distributed along the violin, whereas for SII_R + C_ ACG-Ø most points were at the bottom of the violin showing a consistent reduction from ~400 μm to less than 200 μm. For SII_R, which is the

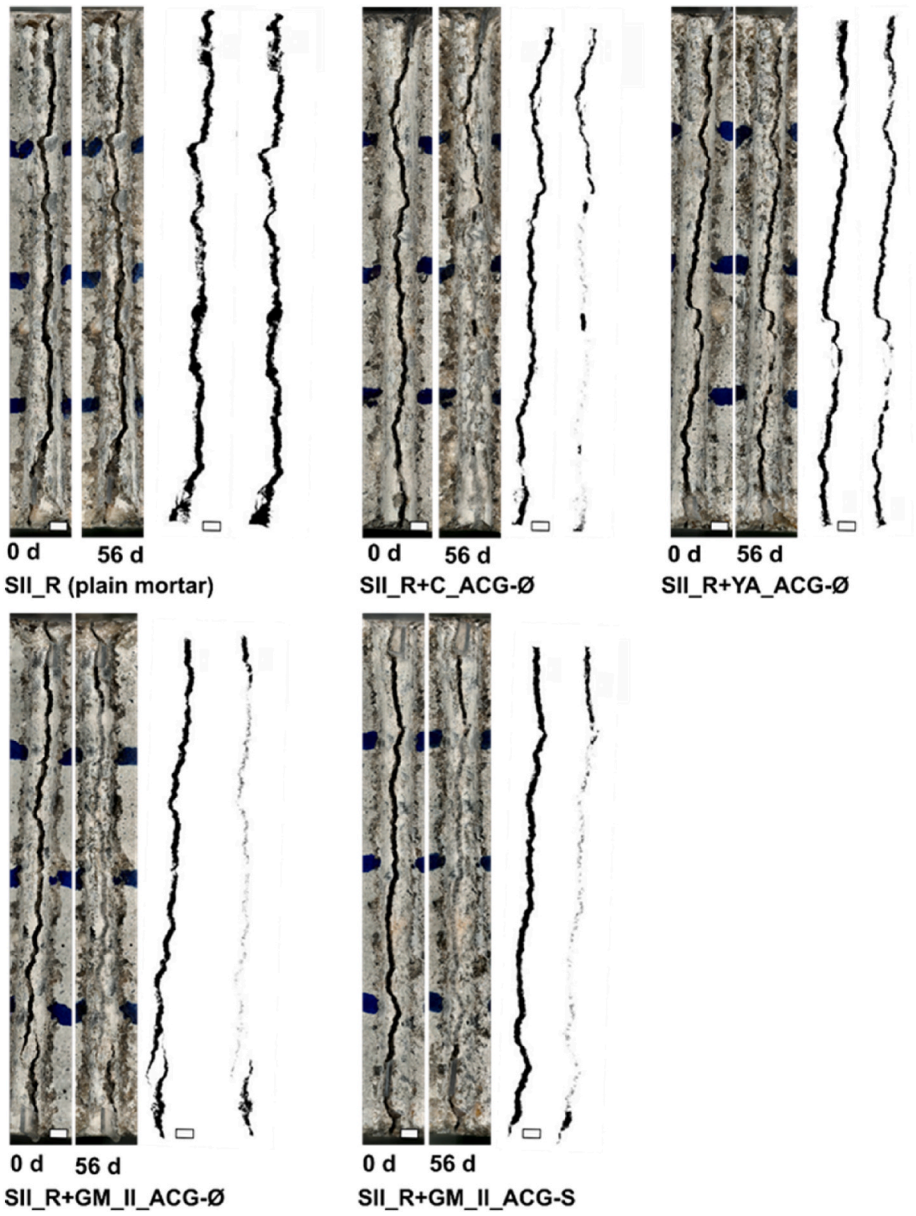

Fig. 4. Original and binarized images of surface cracks of the Set II mortar prisms exposed to tap water for 56 days. A representative mortar prism of each of the five Set II mortar mixes (i.e., SII_R, SII_R + C_ ACG-Ø, SII_R + YA_ ACG-Ø, SII_R + GM_II_ACG-Ø and SII_R + GM_II_ACG-S) is shown at post-cracking (0 d) and after 56 days of healing (56 d). Scale bars represent 1.0 mm.

plain mortar, and SII_R + GM_II_ACG-Ø, only a limited difference can be seen on micro-CT images following 56 days of healing.

To visualise the precipitation within the depth of the crack, pixel intensity was measured at 11 slices across the crack for up to 20 mm depth at Day 0 and Day 56 using micro-CT images (Fig. 9).

The pixel intensity for SII_R + GM_II_ACG-S, SII_R + YA_ ACG-Ø and SII_R increased after 56 days, indicating the deposition of a denser material within the crack. For SII_R + C_ACG-Ø and SII_R + GM_II_ACG-Ø mortar prisms, the density increased slightly at the top surface while no increase was seen within the deeper regions of the cracks, which would correspond to the accumulation of precipitation only at the surface of the crack. Only one mortar prism from each set of triplicates was scanned on micro-CT, so no conclusive results can be made for the particular set of mortar prisms, but it has been shown that micro-CT can be a good method to visualise the crack healing at the surface as well as within the depth of the cracks.

3.4. SEM-EDX and Raman analyses of healing product

The microstructural composition of the healing products was analysed using SEM-EDX and Raman spectroscopy. The SEM images for SII_R (plain mortar) from both the tap water and wastewater showed no deposition of the healing product within the crack. The SEM images of SII_R + GM_II_ACG-S (Fig. 10) containing spores showed almost complete closure of the crack, and the precipitated crystals seem to accumulate from both sides of the crack meeting at the centre. Fig. 11 shows an example of rhombohedral crystals accumulated within the crack. The crystal formation starts from the edges on both sides crack and merges at the centre. The SII_R + GM_II_ACG-Ø mortar prisms (with GM-II and calcium nitrate) kept in wastewater also showed complete closure of the crack with a thin crack of less than 2 μm remaining in the centre. The same samples from tap water showed the formation of crystals around the edges of the crack but not enough to completely close the crack. For the mortars SII_R + C_ACG-Ø and SII_R + YA_ ACG-Ø, partial filling of

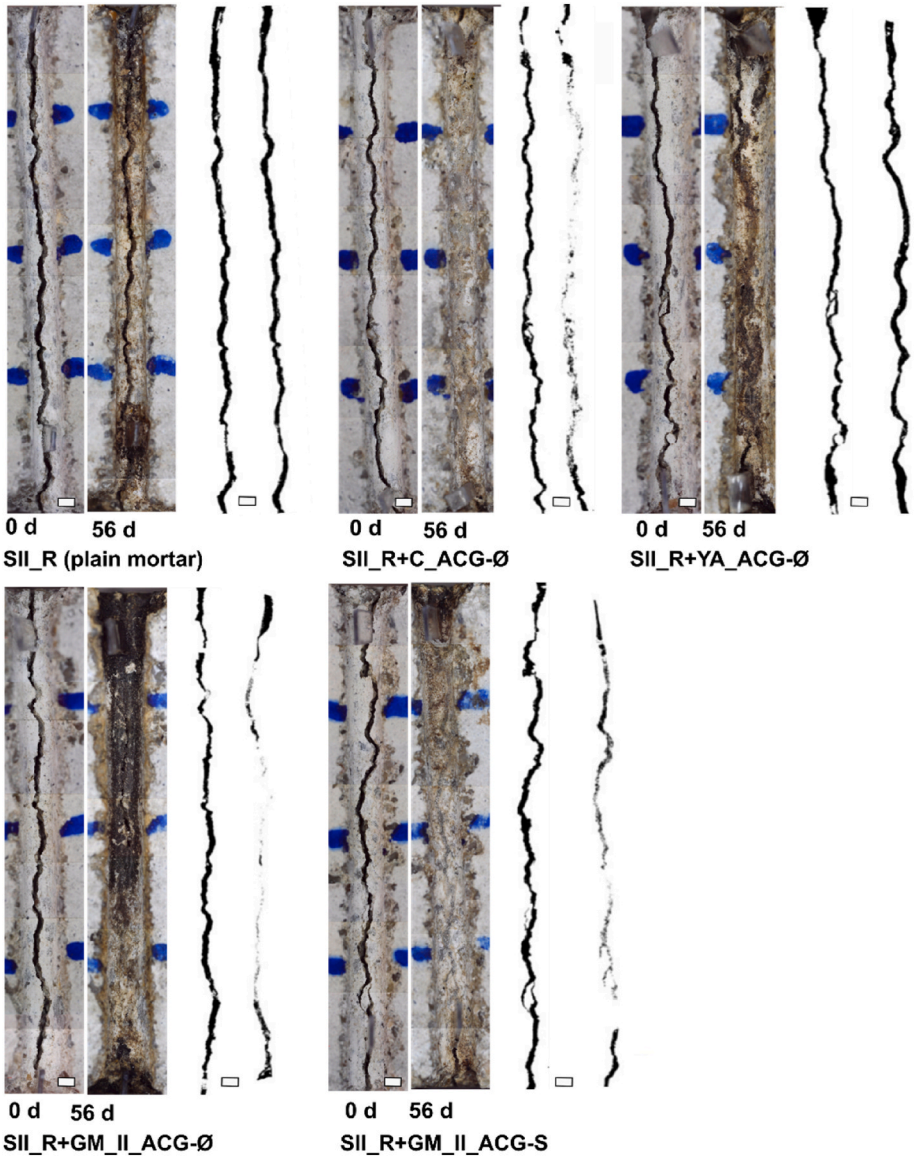

Fig. 5. Original and binarized images of surface cracks of the Set II mortar prisms exposed to wastewater for 56 days. A representative mortar prism of each of the five Set II mortar mixes (i.e., SII_R, SII_R + C_ ACG-Ø, SII_R + YA_ ACG-Ø, SII_R + GM_II_ACG-Ø and SII_R + GM_II_ACG-S) is shown at post-cracking (0 d) and after 56 days of healing (56 d). The regions with darker colour on the right-hand side pictures for each sample (day 56) represent suspended solids, not seen in tap water. Scale bars represent 1.0 mm. (For interpretation of the references to colour in this figure legend, the reader is referred to the Web version of this article.)

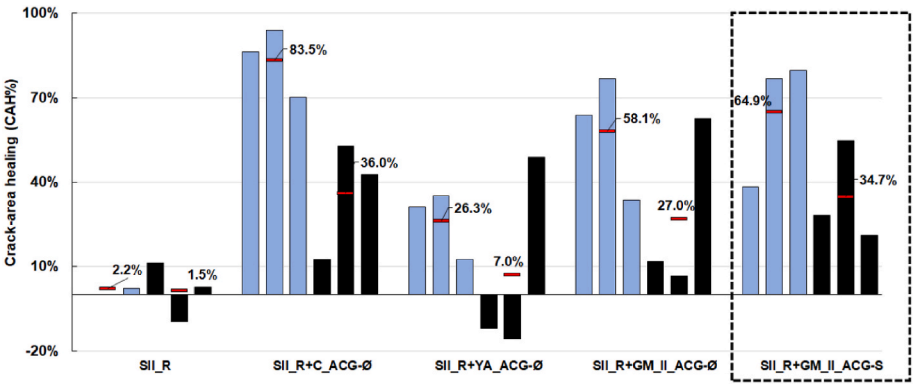

Fig. 6. Crack-area healing percentage (CAH%) for Set II mortar prisms after 56 days of healing. Bars represent the CAH% obtained as a function of crack-area reduction of the individual mortar prisms exposed during the healing period to: (■) tap water and (■) wastewater. The dotted box shows the mortar prisms containing bacterial spores encapsulated into aerated concrete granules (ACGs). Horizontal bars show the average values for each triplet of mortar prisms. The reference mortar mix (SII_R) exposed to tap water comprised only one mortar prism, as the other two prisms were damaged during cracking.

the crack was seen for the samples exposed to wastewater. From the tap-water-exposed mortar prisms, SII_R + C_ACG-Ø also showed healing product at three points in the crack, while SII_R + YA_ ACG-Ø (with only GM-II) showed no healing product in the SEM images. Overall, the wastewater-exposed mortar prisms showed the presence of healing product within the crack in most samples apart from SII_R. This could have been formed by the bacteria present in wastewater on the availability of Ca^{2+} ions and growth media.

The SEM-EDX analysis for SII_R + GM_II_ACG-S and SII_R + GM_II_ACG-Ø mortar prisms (Fig. 12) along the healing product within

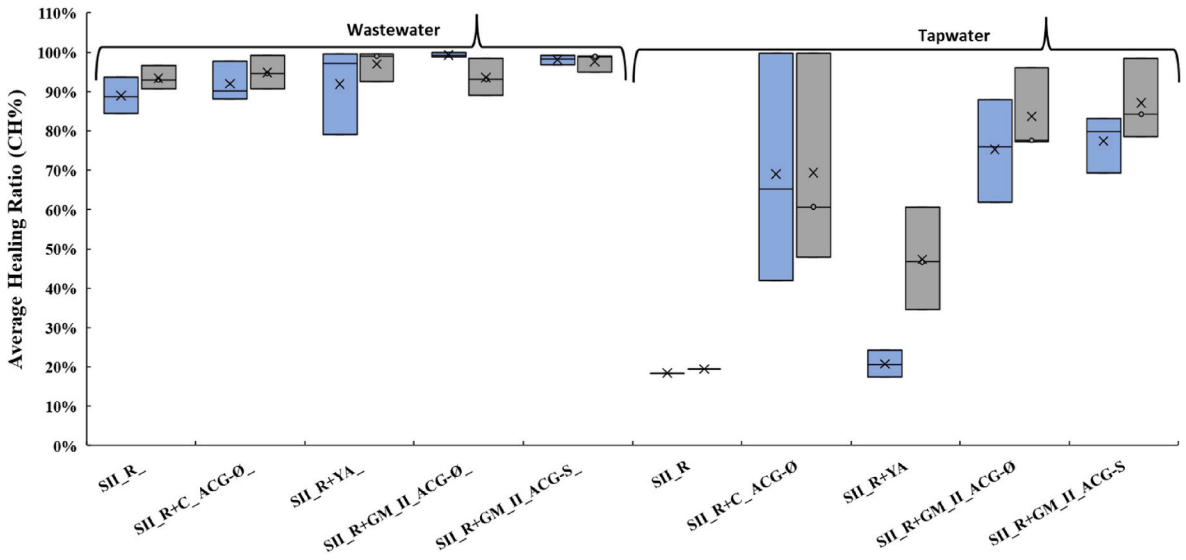

Fig. 7. Boxplot of the crack healing percentage (CH%) as a function of the recovery of the water-tightness after 28 days of healing (■) and 56 days of healing (■). Bottom and top bars of each rectangle represent the minimum and maximum value of each mortar mix, while the middle bar represents the median value. Crosses show the mean value for each triplet of mortar prisms. The reference mortar mix (SII_R) exposed to tap water comprised only one specimen, as the other two mortar prisms were damaged during cracking.

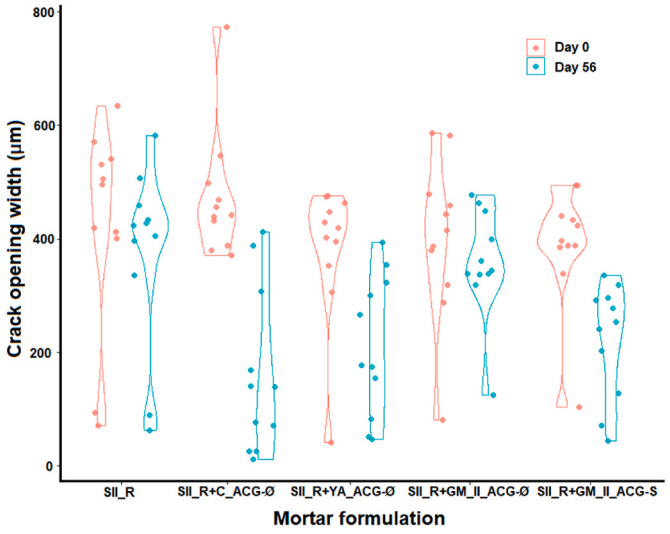

Fig. 8. The crack width changes from Day 0 to Day 56. The comparison is made for 11 points on reconstructed micro-CT images from wastewater-exposed Set II mortar prisms.

the crack shows the presence of C, O and Ca in most abundance, which could be related to the formation of $CaCO_3$ crystals in the crack for both the tap-water and wastewater-exposed mortar prisms. The elemental composition of calcium at different regions of the crack, healing product, and mortar prism was also quantified with SEM-EDX, as represented in Fig. 12. The calcium content at positions a and b in the mortar prisms (Table 2) was the highest, which is due to the high amount of calcium present in cement.

For most of the mortar prisms that showed closure of the crack, the calcium content of the healing product was similar to or higher in the centre of the prisms than on the edges of the crack. The edges of the crack have less calcium content, which could be due to the leaching of Ca^{2+} ions to form calcium carbonate within the crack. This trend was seen in both tap water and wastewater samples with an exception for SII_R + YA_ ACG-Ø and SII_R + GM_II_ACG-Ø mortar prism (Table 2). The chemical composition of the healing product was confirmed through Raman spectroscopy. Raman spectra of the healing product present in the healed cracks of the different mortar prisms presented the four bands that correspond to the Raman spectra of pure calcite [40,41]. Therefore, the healing product within these cracks were confirmed as calcium carbonate ($CaCO_3$) (Fig. 13).

4. Discussion

4.1. Advantages of using sodium acetate as carbon source

The first set of mortar prisms (i.e., Set I) was tested with only yeast extract as the organic carbon source and calcium nitrate as the calcium source with encapsulated CGN12 spores. The formulation has been previously tested with *Bacillus* spores and has shown self-healing of cracks [25]. For the Set II samples, sodium acetate was used as the main organic carbon source [42]. The substitution of the organic carbon source was based on the high cost and negative effects that yeast extract has on the hydration of cement. Yeast extract is also 30-40% more expensive than sodium acetate and compressive strength and setting times are negatively affected by the inclusion of yeast extract. For the former, yeast extract tends to increase air bubbles within the cement matrix and makes cementitious materials more porous, which decreases the overall strength of these materials [25]. For the latter, setting times are extended which could lead to increased construction costs [37–39]. Another advantage of using a defined carbon source, like sodium acetate, is to ensure consistency and reproducibility of the results, as the chemical composition of yeast extract can vary widely between different production lots.

4.2. Comparison of healing in mortar samples

4.2.1. Mortars exposed to tap water

From the CAH% results (Fig. 6), except for the SII_R mortar mix, where the healing observed was negligible (2.2%), the rest of the mortar mixes presented some degree of healing. Moreover, the best healing performance was observed in the three mortar mixes where calcium nitrate was added (CAH% between 58.1% and 83.5%), regardless of whether or not bacterial spores were included. The addition of calcium nitrate results in a higher concentration of Ca^{2+} ions within the mortar matrix that could have resulted in the leaching and building up of these

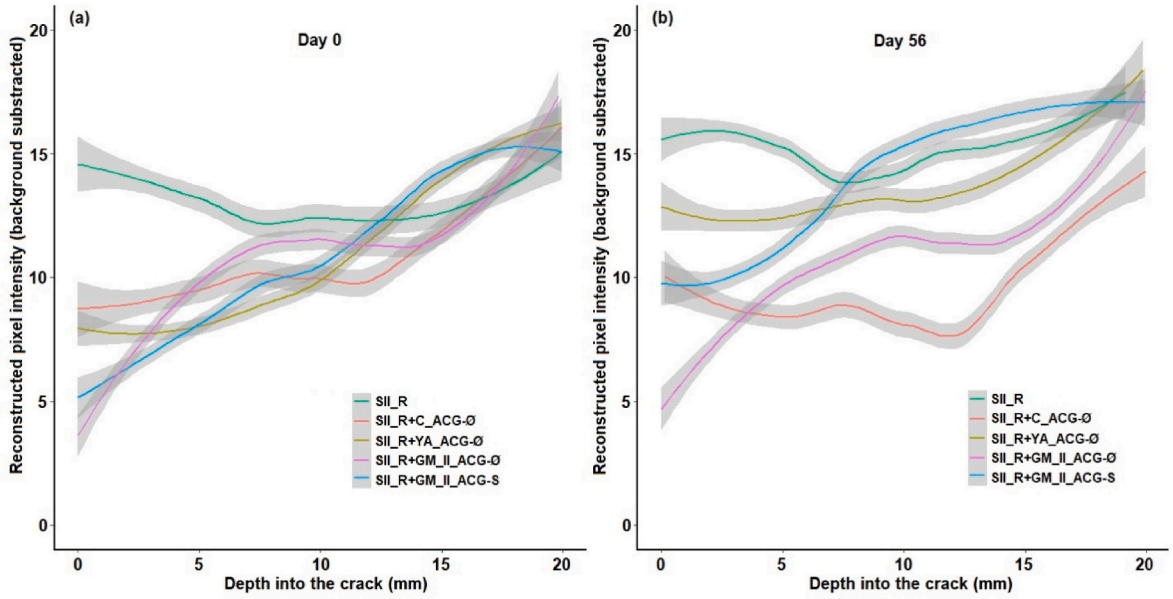

Fig. 9. Mean pixel intensity (from the surface up to 20 mm depth) measured at (a) Day 0 and (b) Day 56 on the micro-CT images for the wastewater-exposed mortar prisms.

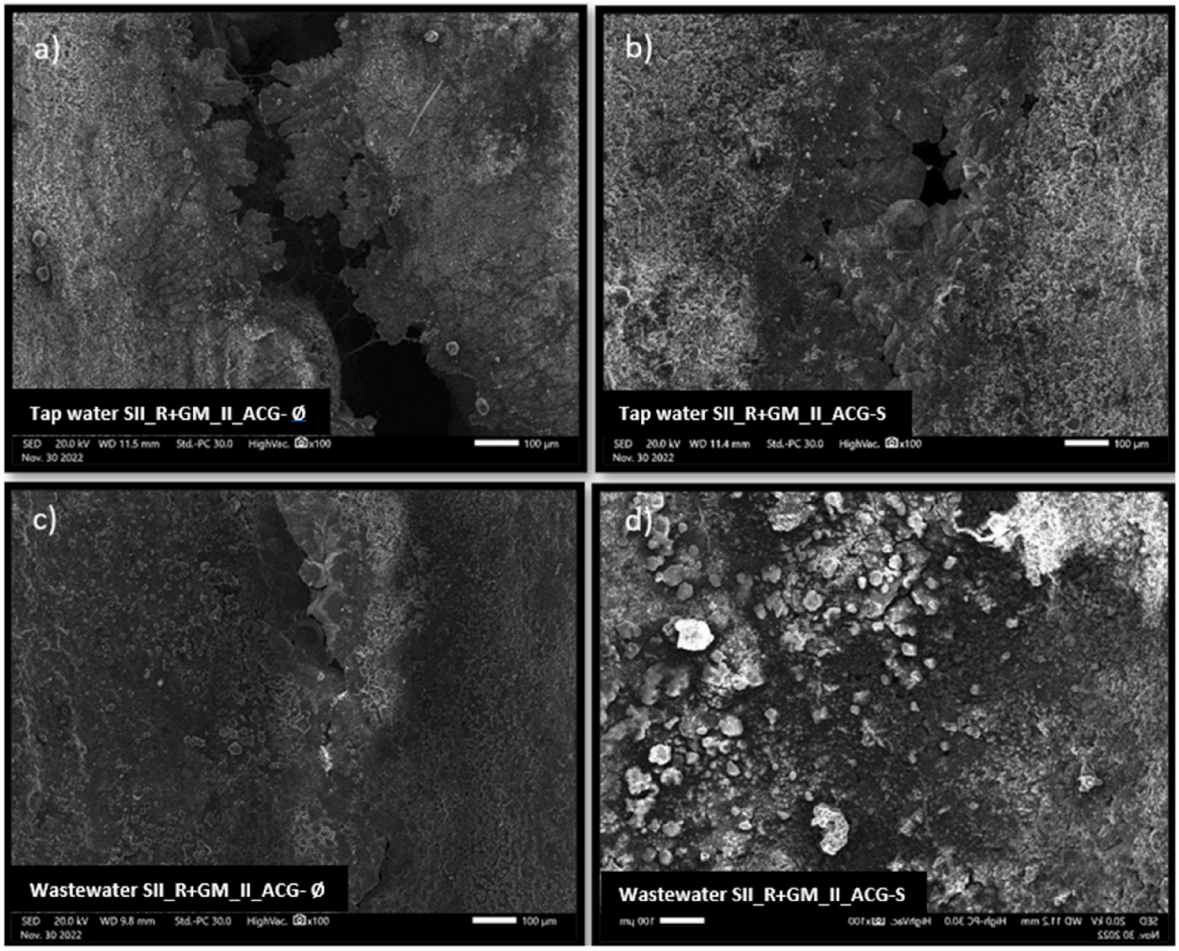

Fig. 10. SEM images of the crack taken after 56 days. Panels a) and b) were obtained from samples without and with spores, respectively, exposed to tap water. Panels c) and d) were obtained from samples without and with spores, respectively, exposed to wastewater.

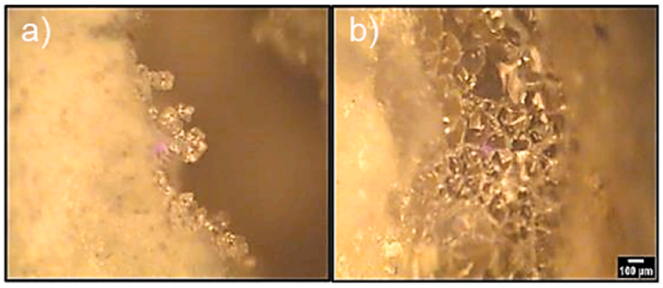

Fig. 11. Example of SEM images depicting rhombohedral crystal formation within the crack. a) TW_SII_R + GM_II_ACG-Ø; b) WW_SII_R + YA_ ACG-Ø.

ions within the cracks. Then, once a supersaturated calcium condition was reached, calcium hydroxides precipitated and, in the presence of atmospheric CO_2, were converted into calcium carbonates. However, the two mortar mixes containing both calcium nitrate and sodium acetate (i.e., SII_R + GM_II_ACG-Ø and SII_R + GM_II_ACG-S) presented very similar crack-area healings to each other, but significantly lower than the mortar mix containing only the calcium nitrate but no sodium acetate (i.e., SII_R + C_ACG-Ø). This lower healing efficiency likely is the result of the presence of sodium acetate in the cement matrix. The addition of sodium acetate to cement mortars results not only in an increase of interfacial bonds (-CH) between hydration products and sand grains [43] but also in the formation of hydrophobic organosilicon bonds (C-Si) inside the capillary pores [43], both mechanisms leading to a denser and less permeable cement matrix [44,45]. In this regard, fewer Ca^{2+} ions were likely able to migrate from the cement matrix resulting in fewer precipitates formed within the crack. For the mortar mix where sodium acetate was available, but no calcium nitrate or bacterial spores were added (i.e., SII_R + YA_ACG-Ø), the average CAH% observed (26.3%) was considerably lower than the observed for the three calcium-added mortar mixes (with and without bacterial spores). A possible explanation could be the presence of naturally occurring bacteria that, in combination with the available sodium acetate and the presence of dissolved Ca^{2+} ions (from cement matrix and tap water), could have contributed to the observed healing, as tap water and non-sterile conditions were used in this study to reproduce real-life conditions. Important to mention is that the SII_R + YA_ACG- Ø mix differs from the reference mix (SII_R) only in the availability of sodium acetate within the cement matrix. Therefore, as no organic carbon source was purposely added to SII_R mortar prisms, environmental bacteria were not likely able to induce calcium precipitation within the cracks, thus resulting, as expected, in the negligible CAH% observed

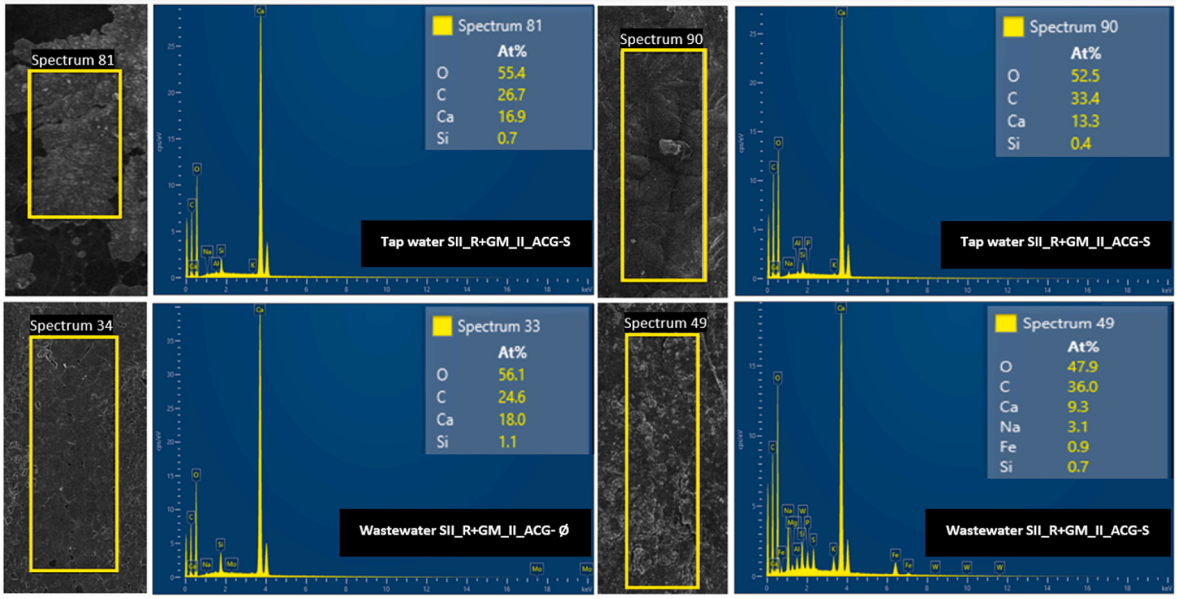

Fig. 12. Example of EDX spectra showing different elements present within the healing product precipitated within the crack for the selected mortar samples and healing conditions.

Table 2
Calcium content (%) at different regions on the mortar prisms as measured with SEM-EDX.

Measurement point on the prism	Centre		Left hand side of the crack			Right hand side of the crack			On the crack		
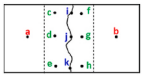	a	b	c	d	e	f	g	h	i	j	k
Mortar formulation											
TW_ SII_R	14.8	15.6	14.6	1.0	7.4	4.3	13.2	9.7	–	–	–
TW_ SII_R + C_ ACG-Ø	14.3	13.6	9.7	8.8	13.7	3.4	8.4	16	14.8	17.2	17
TW_ SII_R + YA_ ACG-Ø	13.6	12.8	7.9	2.6	4.2	4.5	5.2	4.3	–	–	–
TW_ SII_R + GM_II_ACG-Ø	12.9	12.8	2.0	3.3	6.8	4.4	6.1	5.9	13.8	16.9	15.7
TW_ SII_R + GM_II_ACG-S	14.6	15.0	3.8	2.8	5.6	4.0	4.0	5.0	14.6	13.3	15.9
WW_ SII_R	16.2	15.7	13.3	11.2	12.0	8.4	5.5	7.5	–	–	–
WW_ SII_R + C_ ACG-Ø	13.3	15.5	8.7	9.3	8.4	12.2	13.2	5.9	17.6	5.4	9.8
WW_ SII_R + YA_ ACG-Ø	14.8	14.5	8.5	36.5	7.2	9.9	35.8	25.4	35.8	39.2	6.4
WW_ SII_R + GM_II_ACG-Ø	16.1	13.8	16.7	16.7	16.5	16.2	18	17.1	17.2	18.1	17.5
WW_ SII_R + GM_II_ACG-S	14.1	16.1	5.2	6.5	5.5	6.5	8.7	8.1	11.3	9.3	8.6

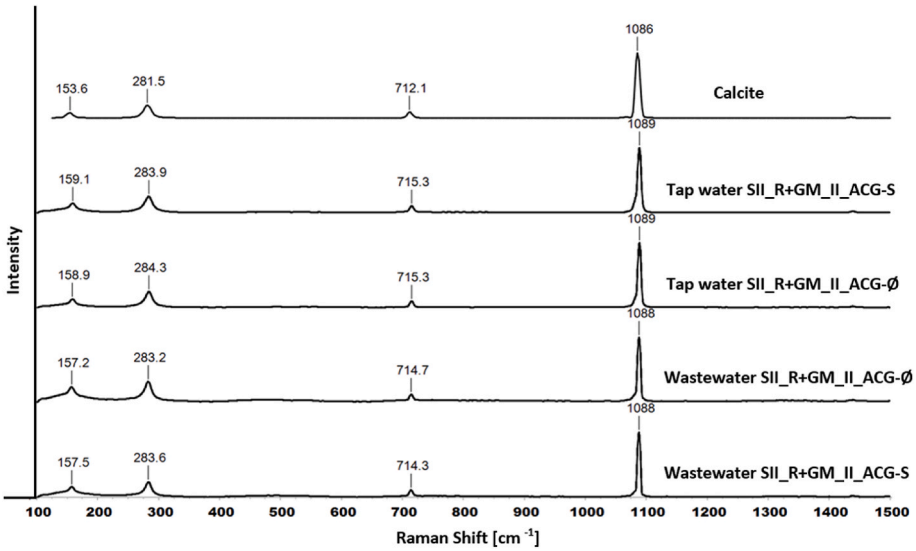

Fig. 13. Raman spectra of the healing precipitates formed within the cracks of SII_R + GM_II_ACG-Ø (without spores) and SII_R + GM_II_ACG-S (with spores) mortar prisms after being exposed to tap water or wastewater healing conditions. The four main peaks observed on the four mortar mixes correspond to the Raman spectra of pure calcite [40,41].

(2.2%).

However, if the information from the visual quantification of the crack healing is complemented with the results observed after 56 days of healing as a function of the recovery of the water tightness (Fig. 7), then a better understanding and interpretation of the healing efficiency can be achieved. Water-tightness recovery results show a higher and more consistent healing (i.e., mean healing (%): 83.7–87.1%, coefficient of variation: 0.09–0.11, for SII_R + GM_II_ACG-S and SII_R + GM_II_ACG-Ø, respectively) is observed for the two mortar mixes containing both the calcium nitrate and the organic carbon source, where the difference among these two mixes was the addition or not of bacterial spores. The more effective water-tightness recovery of these two mortar mixes could likely be attributed to the presence of bacteria within the crack, either purposely added (CGN12) or naturally present in the environment, as the conditions necessary for achieving MICP were likely fulfilled (i.e., carbon source, additional calcium source, water and oxygen) [15,46]. On the other hand, significantly lower and less consistent healing (i.e., mean healing (%): 69.4%; CV: 0.32) was observed for the mortar mix containing calcium nitrate, but no organic carbon source (SII_R + C_ACG-Ø). Therefore, the healing observed in this mortar mix could likely result from the precipitation of calcium hydroxide crystals and their subsequent transformation into carbonates due to their exposure to atmospheric CO_2 [25]. In contrast, a very low water-tightness recovery was observed for SII_R (plain mortar mix) and SII_R + YA_ACG-Ø, with 19.4% and 47.3% mean healing values, respectively. The results observed for SII_R + YA_ACG-Ø confirm that for having MICP, either from the bacteria purposely embedded or from environmental bacteria, the Ca^{2+} ions that could be available from the mortar matrix alone are not enough to achieve proper healing.

4.2.2. *Mortars exposed to wastewater*

Similar to the results observed for the equivalent mortar mixes exposed to tap water, the three mortar mixes containing an additional source of calcium presented the best healing in wastewater when the reduction in the crack area was quantified (Fig. 6). However, all the crack-area healing percentages achieved by the wastewater-exposed mortar prisms were significantly lower than the percentages observed for the tap-water-exposed mortar prisms. In this regard, one of the big challenges of evaluating the healing performance via the visual quantification of the crack area when samples are exposed to a continuous wastewater flow comes from the inherent presence of a significant amount of suspended solids. Even though mortar prisms were, before taking the microscope images, gently cleaned with tap water to remove as many adhered solids as possible without damaging any healing product within the crack, a 100% crack area free of adhered solids was not feasible. As these attached solids have a dark colouration, the pixel values can be cofounded between the pixels representing the darker colours of the mortar matrix and these dark pixels representing the attached solids. Derived from this, the results obtained from the crack-area healing quantification for samples exposed to the conditions mentioned above must be taken with caution. Nevertheless, it is possible to better understand the healing performance of the different wastewater-exposed mortar prisms when the visual analysis is qualitative and, thus, does not rely on the analysis software to calculate the crack area reduction. No precipitates were visually observed within the cracks of the wastewater-exposed mortars when no calcium precursor was included in the mix (i.e., SII_R and SII_R + YA_ ACG-Ø). For the SII_R + C_ACG-Ø mortar prisms, microscope images showed less overall healing when compared to equivalent samples exposed to tap water. It is hypothesised that the accumulation of solids within the crack at an early age could likely have influenced the precipitation of Ca^{2+} ions, either originated from the cement matrix or available from the wastewater.

On the other hand, wastewater-exposed specimens of SII_R + GM_II_ACG-Ø showed the formation of more healing product within the crack than the equivalent tap-water-exposed mortar specimens (Fig. 14).

Wastewater, on its own, is a rich source of soluble minerals (including calcium), organic matter and microorganisms. The healing of cracks for SII_R + GM_II_ACG-Ø samples in wastewater could be attributed to the abundant bacteria inherently present in wastewater (see Appendix B). While we cannot attribute the observed healing activity to a particular group of bacteria in the wastewater, it is interesting to note that the second largest group present in the metagenome analysis was the Terribacteria Group, which includes the type of bacteria (Bacilli, including the strain CGN12 used here, and Sporosarcina), which are most commonly used in self-healing concrete applications. The interior of the crack likely presented favourable conditions for the establishment of bacterial communities, which in the abundant presence of organic matter and availability of Ca^{2+} ions, could plausibly have led to calcium carbonate precipitation. In a similar way, but with more restricted access to a carbon source and Ca^{2+} ions, environmental bacteria could have contributed to the formation of healing product within the cracks of tap-water-exposed mortars. However, not only the limited amount of

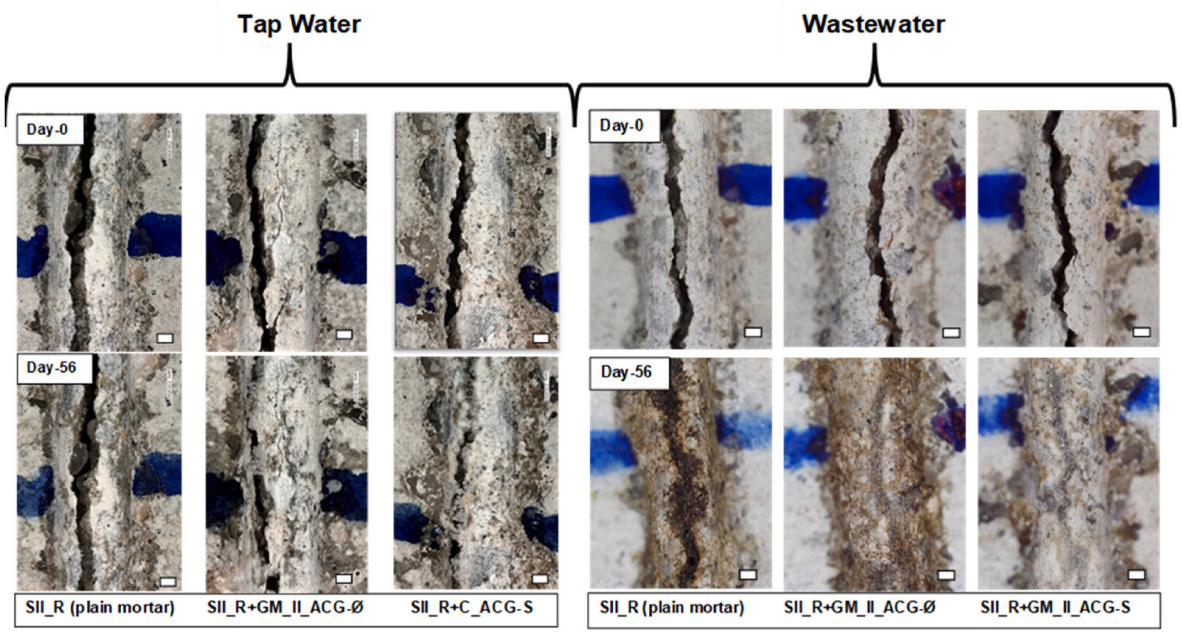

Fig. 14. Representative samples of SII_R, SII_R++GM_II_ACG-Ø and SII_R + GM_II_ACG-S immediately after cracking (i.e., Day-0) and after 56 days of being exposed to tap water (*Left)* and wastewater *(Right)*. Each image corresponds to the middle point marked with a permanent pen. The scale bar represents 0.50 mm.

carbon and calcium sources available in the tap water when compared to wastewater but also the significantly less diverse natural bacterial community likely resulted in the less efficient healing observed in the cracks of tap-water-exposed mortar prisms. Wastewater-exposed SII_R + GM_II_ACG-S mortar prisms showed more efficient healing when compared to equivalent tap-water-exposed samples (Fig. 14). In this regard, all three SII_R + GM_II_ACG-S mortar prisms showed complete crack closure, while the tap-water-exposed mortar prisms did not show the same consistent results. Both sets of mortar prisms contained encapsulated spores, which likely germinate when exposed to favourable conditions and induce calcium carbonate precipitation. Nevertheless, no consistent and sufficient precipitation was observed on the wastewater-exposed mortar prisms that lacked the combined addition of calcium nitrate and sodium acetate (i.e., SII_R, SII_R + YA_ ACG-Ø and SII_R + C_ ACG-Ø). Therefore, addition of calcium nitrate and sodium acetate proved effective in inducing calcium carbonate precipitation, not only for the samples with bacteria purposedly added, but also for the samples which are only exposed to the environmental bacteria naturally present in wastewater. In this context, recent studies have demonstrated that heterotrophic bacteria present in wastewater are able to induce calcium carbonate precipitation [47] and that biomineralisation has been successfully used to remove Ca^{2+} ions from wastewater *via* the use of ureolytic bacteria [48,49].

Furthermore, when the results obtained from the water-tightness recovery tests were analysed (Fig. 7), it was observed that the five mortar mixes showed almost complete healing after 56 days of being exposed to a wastewater flow. However, these results have to be taken with caution, as discussed above for the results obtained using crack-area quantification. In this regard, the results could likely be influenced by the presence of suspended solids accumulated deep inside the cracks, which could have resulted in the reduction of the water-flow coefficient. For future studies requiring water-tightness recovery of wastewater-exposed samples where significant accumulation of suspended solids is anticipated, alternative water permeability setups could be considered [34]. These setups may involve water flow from the inside of the sample to the outside through the crack or utilising complete cracks, which would aid in the removal of deposited particles. Such alternative setups are anticipated to produce more uniform water-flow results when evaluating water tightness recovery of self-healing samples exposed to these conditions.

Nevertheless, it was observed that a more consistent and improved water-tightness recovery value was obtained for SII_R + GM_II_ACG-Ø and SII_R + GM_II_ACG-S mortar mixes. These results suggested that by providing additional calcium and organic carbon sources together, better environmental conditions within the crack were available for either purposely added bacteria or environmental bacteria when the samples were exposed continuously to a wastewater flow. The additional nutrients and calcium embedded within the cement matrix likely allowed bacteria naturally present in the wastewater to achieve some degree of healing on cracks less than 0.5 mm in width. However, when calcite-forming bacteria were purposely included in these cementitious materials, efficient healing was obtained. In this context, a recent study [50] reached a similar conclusion when cement mortars containing vegetative *Bacillus sphaericus* immobilised in diatomaceous earth were exposed to wastewater during a 90-day healing period. They concluded that the nutrients present in the wastewater aided purposely added bacteria to successfully induce calcium carbonate precipitation.

In summary, for samples exposed to municipal wastewater, it was observed that the use of BBSH cementitious materials results in effective crack healing. However, even if bacterial spores are not purposely added to these cementitious materials, as long as an organic carbon source (i.e., sodium acetate) and abundant Ca^{2+} ions are present within the cement matrix, it was observed that reasonable healing can be achieved due to the activity of bacteria naturally present in the wastewater. In this regard, if a rich and abundant environmental bacteria community is not present, as in the case of tap water, then even though the required organic carbon and calcium sources are supplied, efficient healing will likely not be achieved.

The findings of this study open the door for the production of bespoke BBSHCs. The production and encapsulation of bacterial spores is a complex and expensive process [51]. Nevertheless, bacterial spores are crucial and need to be included in concrete structures that will be exposed to water where a low and not diverse bacteria community is present (e.g., tap water, rainwater, etc.). However, for wastewater infrastructure applications, the abundant rich bacteria community inherently present in wastewater can assist in inducing calcium carbonate precipitation as long as an organic carbon source and enough Ca^{2+} ions are readily available within the cement matrix. In this context,

by eliminating or significantly reducing the bacterial spores needed for BBSHCs designed to be exposed to wastewater, a more economic and straightforward process to produce BBSHC can be achieved. Nevertheless, further research needs to be conducted to optimise these wastewater exposed BBSHCs.

4.3. Microstructural analyses

The size of the mortar prisms used in this study was compatible with the SEM-EDX and Raman instruments, which was a major advantage as we could to confirm the nature of the healing product and its chemical composition without destructing the samples. The SEM images show that the precipitation starts to occur from the edges of the crack, grow towards the centre and, if enough healing product is formed, eventually results in the complete closure of the cracks, as also reported in Ref. [25]. The EDX and Raman spectroscopy further confirmed that the crystals formed were of calcium carbonate in the calcite morphology (Fig. 13). The reaction between the calcium salt present in the mortar with the CO_2 released by bacterial metabolism leads to the formation of insoluble calcium carbonate in the cracks and this healing the cracks. The control mortars also showed precipitation within the cracks which is similar to the results reported in Ref. [52], with formation of $CaCO_3$ crystals in samples with bacteria as well as in control samples. The EDX results reported in Ref. [25] showed more calcium in the precipitate with the samples having bacteria. In the current study more calcium can be seen in the mortar prisms with bacteria purposely added, for both tap water and wastewater samples [22,25,52–55].

The amount of elemental calcium was measured at different regions of the mortars. For most of the samples, wherever the precipitation occurred within the crack, the amount of elemental calcium within the precipitate was high or almost equal to the mortar prisms while less on the left- and right-hand side of the cracks. This is due to the diffusion of Ca^{2+} ions in the presence of water from a region of supersaturation to the cracks within the mortars and which is why less calcium was present on the edges of the cracks as it was used up by bacterial cells to form calcium carbonate precipitate. The amount of elemental calcium measured using SEM-EDX at different regions of the mortar prisms confirms the migration of calcium ions within the mortar prisms [56].

For the current study, microscopic images have given the most conclusive results for the crack healing efficiency for different types of mortar samples in tap water and wastewater. The drawback of microscopic imaging is that it does not give any information about the spatial organisation beyond the surface. For this reason, micro-CT analysis was used as a non-destructive method to visualise the healing within the depth of the crack. Two types of analysis were done using the reconstructed micro-CT images of Day 0 and Day 56 mortars with separate references manually to visualise the precipitation within the crack [57]. The crack width was compared from Day 0 to Day 56, which was found to reduce for all the mortar prisms. The results show that micro-CT can be a good method to visualise the precipitation within the deeper region of the cracks. Due to the brittle nature of the cement, cutting the mortar would disturb the newly formed precipitate. ImageJ was used for the analysis of the reconstructed micro-CT images, which is an easy-to-use software and can give quantitative results from the micro-CT images. Though the disadvantage of micro-CT is that the density of the newly formed material is similar to the mortar prisms, which has to be considered while processing the images to use different thresholds.

5. Conclusions

The purpose of this study was to explore the feasibility of using BBSHCs during the construction of wastewater treatment plants (WWTPs) with the aim of increasing the durability of these concrete structures. The following key conclusions can be drawn:

1. Crack-area quantification using binarized images has been successfully used to visually evaluate the healing efficiency of mortar samples when these are incubated in controlled laboratory conditions (i.e., tap water). However, when mortar prisms are exposed to a continuous wastewater flow for a long period of time (i.e., 56 days), this analysis method is not reliable as a significant amount of the suspended solids can be deposited within the crack, resulting in cofounded pixel values.
2. Bacterial spores are crucial and need to be included in BBSHC exposed to tap water where a bacterial community of less abundance and diversity is present (as compared to municipal wastewater) to perform metabolic activity leading to calcium carbonate precipitation.
3. For BBSHC applications in wastewater infrastructure, the abundant rich bacteria community inherently present in wastewater can effectively induce calcium carbonate precipitation as long as a combination of an organic carbon source (sodium acetate or yeast extract) and enough Ca^{2+} ions are readily available within the cement matrix. This finding has the potential to significantly reduce costs and simplify the production process of BBSHCs for this specific application.

CRediT authorship contribution statement

Manpreet Bagga: Conceptualisation, Formal analysis, Investigation, Methodology, Visualisation, Writing – original draft. **Ismael Justo-Reinoso:** Conceptualisation, Formal analysis, Investigation, Methodology, Visualisation, Writing – original draft. **Charlotte Hamley-Bennett:** Investigation, Writing – review & editing. **George Merces:** Formal analysis, Methodology, Writing – review & editing. **Saimir Luli:** Formal analysis, Methodology, Writing – review & editing. **Ange Therese Akono:** Formal analysis, Methodology, Writing – review & editing. **Enrico Masoero:** Conceptualisation, Writing – review & editing. **Kevin Paine:** Conceptualisation, Supervision, Writing – review & editing. **Susanne Gebhard:** Conceptualisation, Funding acquisition, Project administration, Supervision, Writing – review & editing. **Irina D. Ofiţeru:** Conceptualisation, Funding acquisition, Project administration, Supervision, Writing – review & editing.

Funding

This work was funded by EPSRC Standard Grant *Engineering Microbial-Induced Carbonate Precipitation via Meso-Scale Simulations* (eMICP) (Newcastle University EP/S013997/1; University of Bath EP/S013857/1; Cardiff University EP/S01389X/1).

Declaration of competing interest

The authors declare that they have no known competing financial interests or personal relationships that could have appeared to influence the work reported in this paper.

Data availability

All data created during this research is openly available from Newcastle University Research Data Archive at https://doi.org/10.25405/data.ncl.c.6638210.

Acknowledgements

We acknowledge the support of Dr Isabel Arce Garcia, Scientific Officer in the Electron Microscopy and Analysis Unit. We thank Prof Anil Wipat for the metagenome data analysis. We thank Northumbrian Water Ltd for access to BEWISe pilot plant facility.

Appendix A. Crack generation setup and microscope verification process

Cracking generation via three-point bending. Carbon fibre-reinforced polymer (CFRP) strips were affixed to guarantee the integrity of the mortar prisms after cracking.

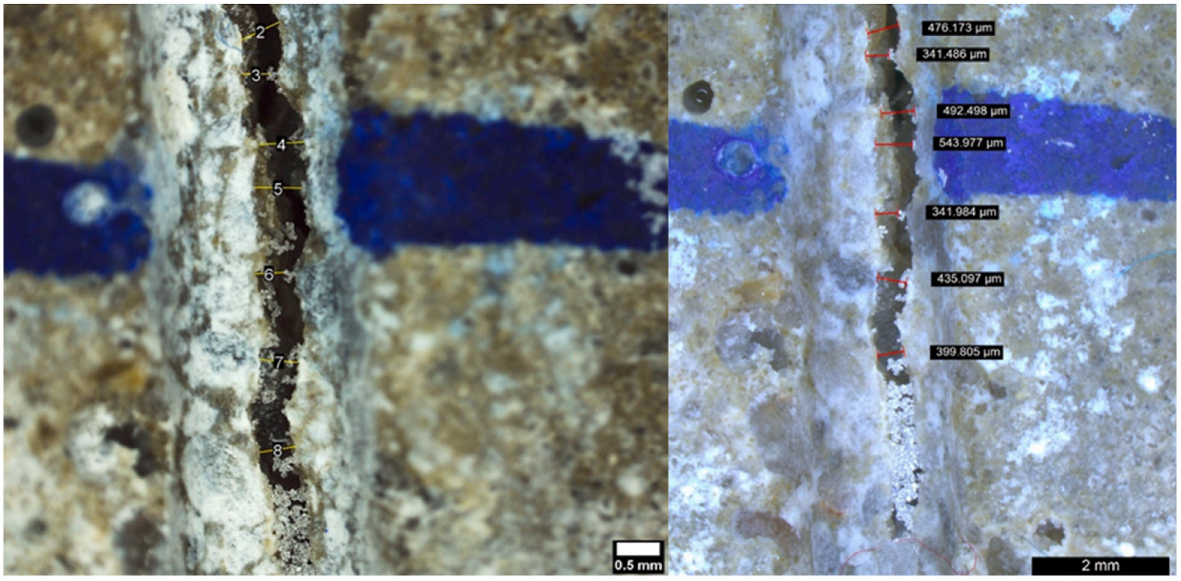

Verification process comparing the accuracy levels of the two microscopes used in this study, namely Celestron (***left***) and Keyence (***right***)), to ensure similar levels of accuracy between them.

Comparative measurements for microscope Celestron (A) and Keyence (B)			
Location	A (µm)	B (µm)	Difference (%)
2	0.470	0.476	−1.3
3	0.334	0.342	−2.4
4	0.507	0.493	2.8
5	0.532	0.544	−2.3
6	0.332	0.342	−3.0
7	0.443	0.435	1.8
8	0.411	0.400	2.7

Appendix B. Wastewater metagenome composition

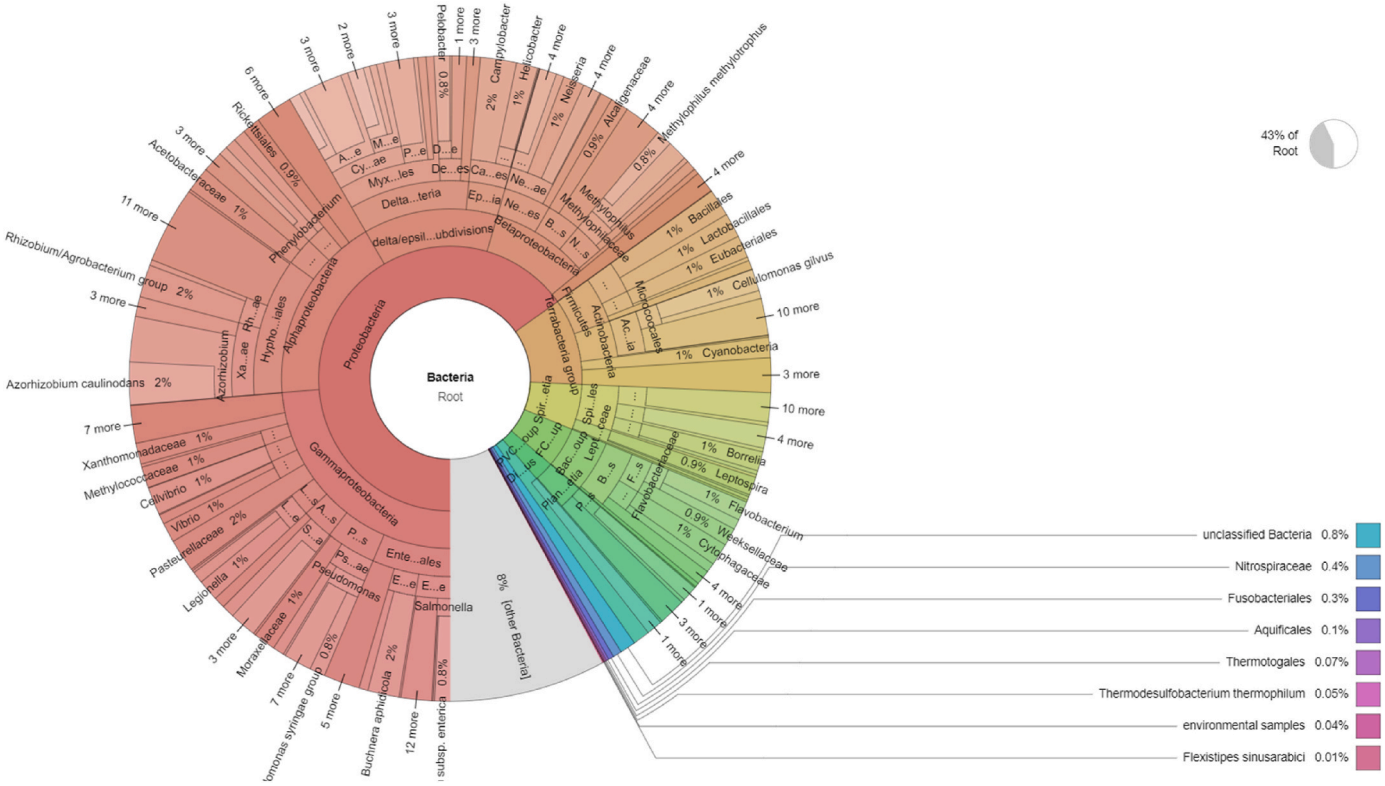

Krona metagenomic visualisation for the bacterial community in the sample collected from the tap.

Krona metagenomic visualisation for the bacterial community in the sample collected from the tray.

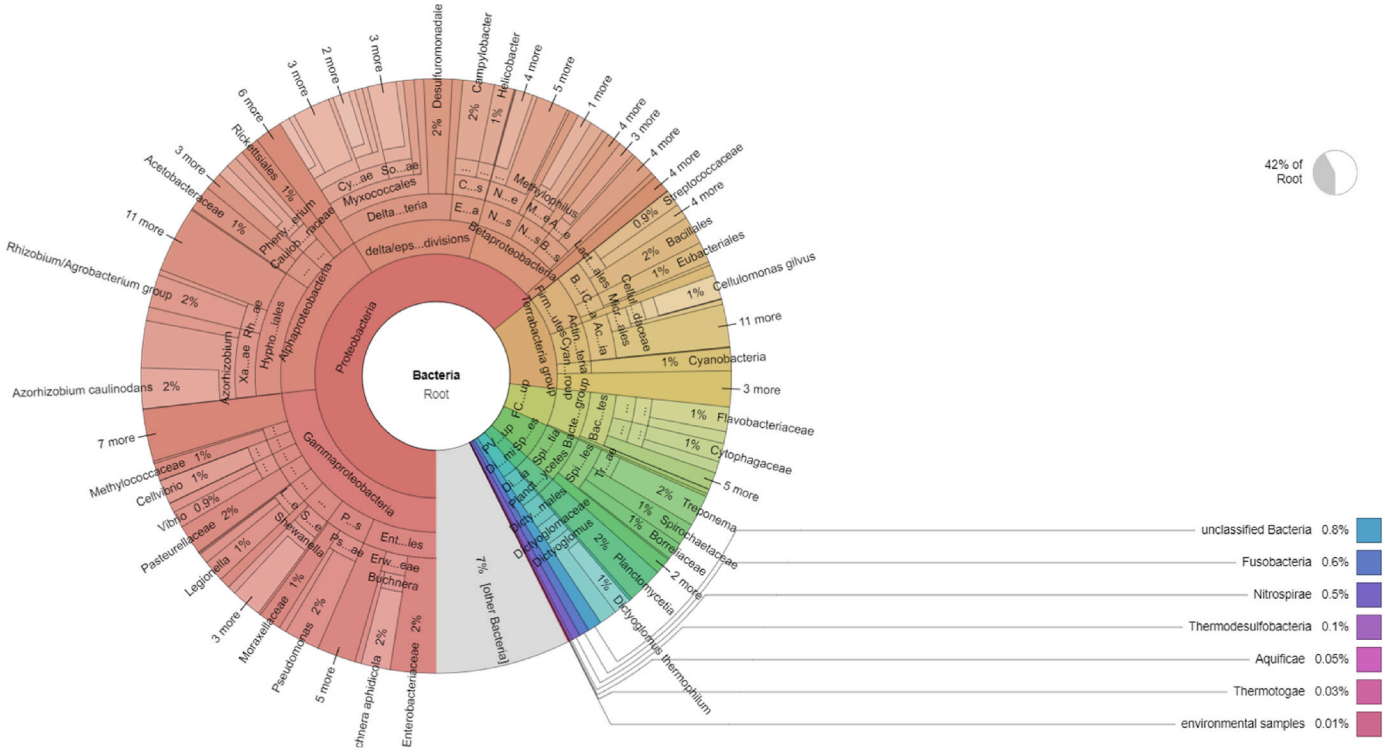

Appendix C. Crack area quantification

Samples exposed to tap water (Set I)

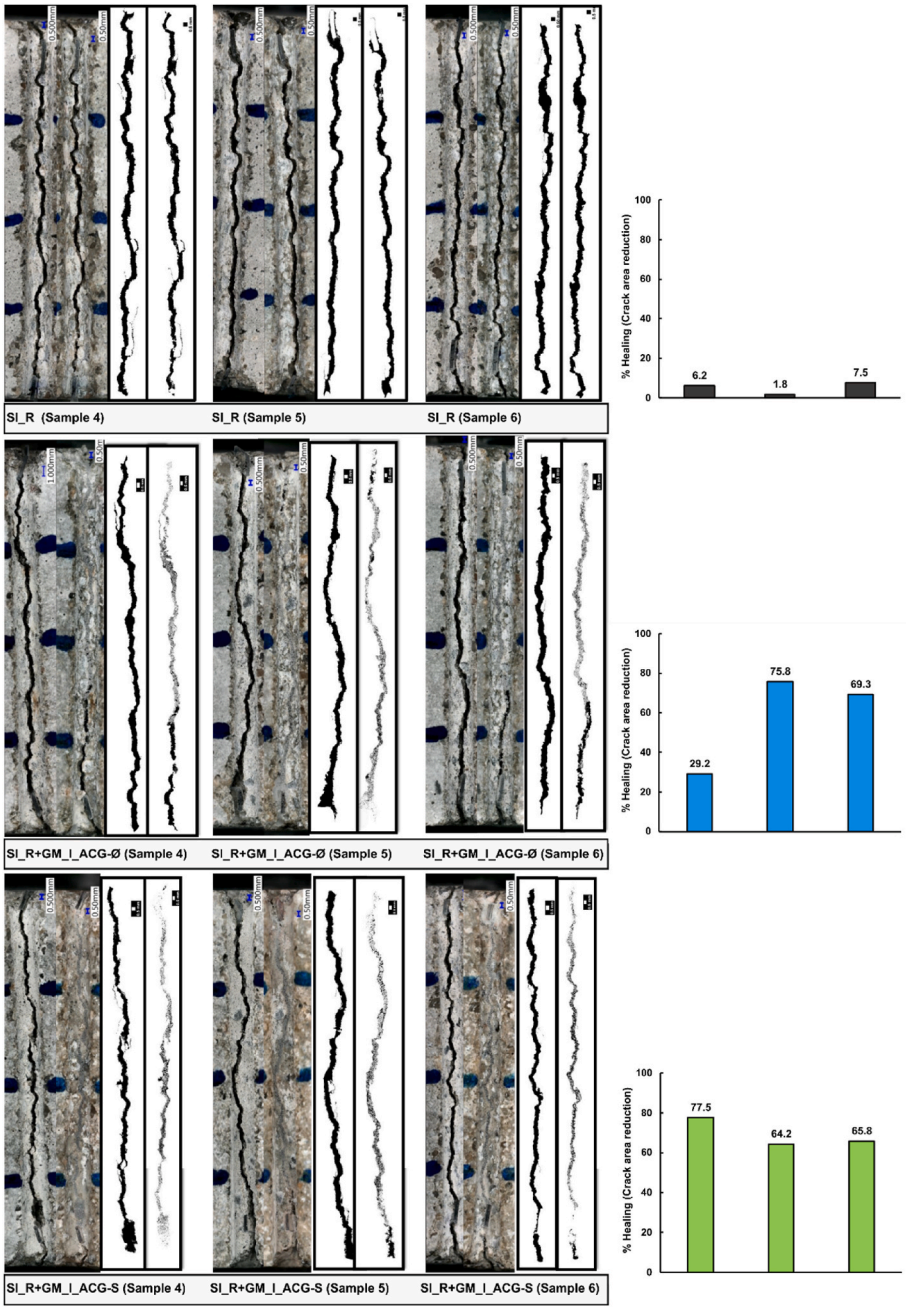

Samples exposed to wastewater (Set I)

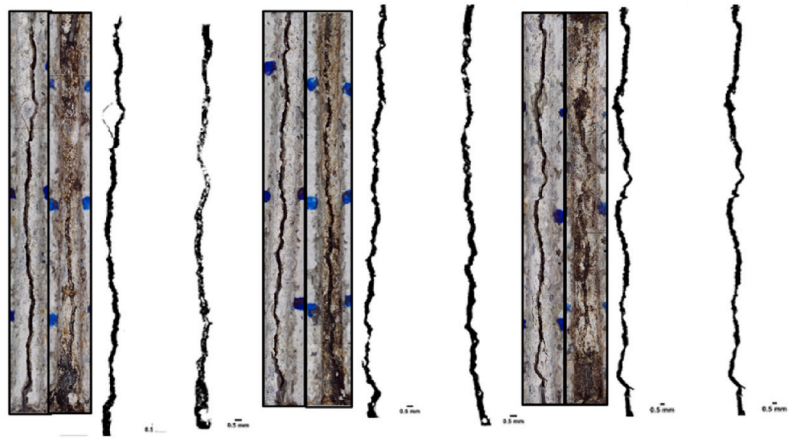

SI_R (Sample 1) SI_R (Sample 2) SI_R (Sample 3)

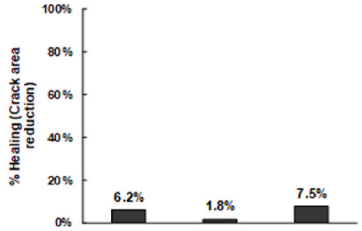

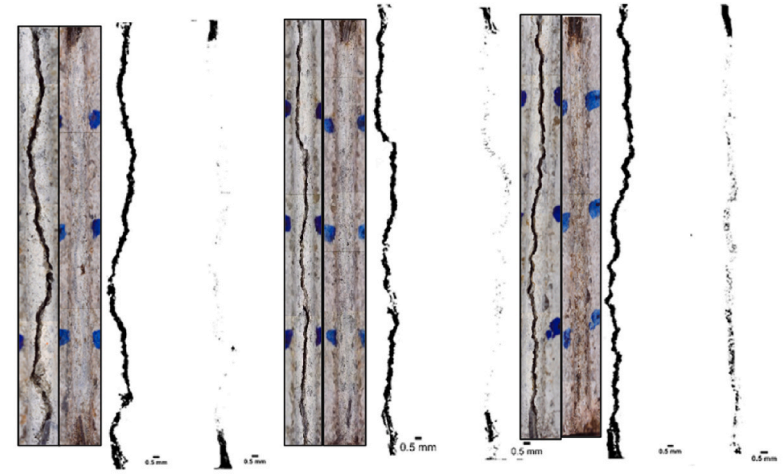

SI_R+GM_I_ACG-Ø (Sample 1) SI_R+GM_I_ACG-Ø (Sample 2) SI_R+GM_I_ACG-Ø (Sample 3)

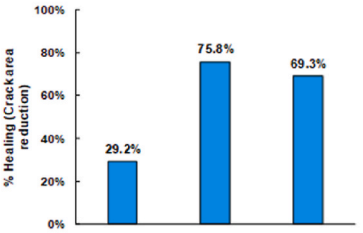

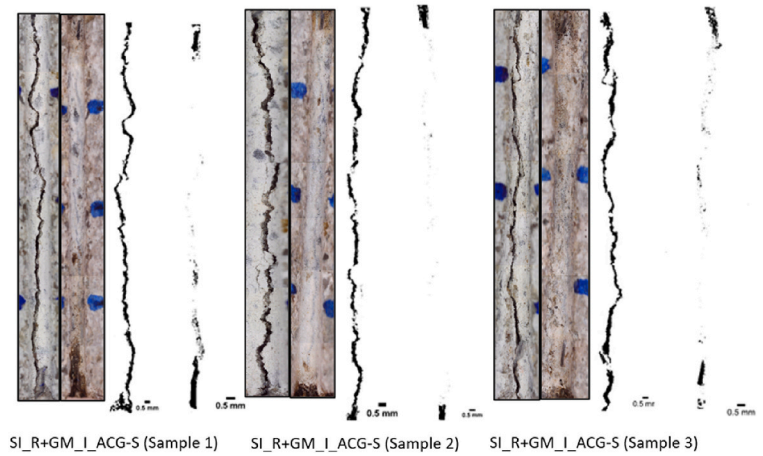

SI_R+GM_I_ACG-S (Sample 1) SI_R+GM_I_ACG-S (Sample 2) SI_R+GM_I_ACG-S (Sample 3)

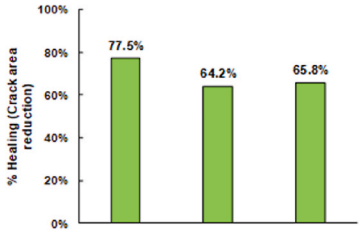

Samples exposed to tap water (Set II)

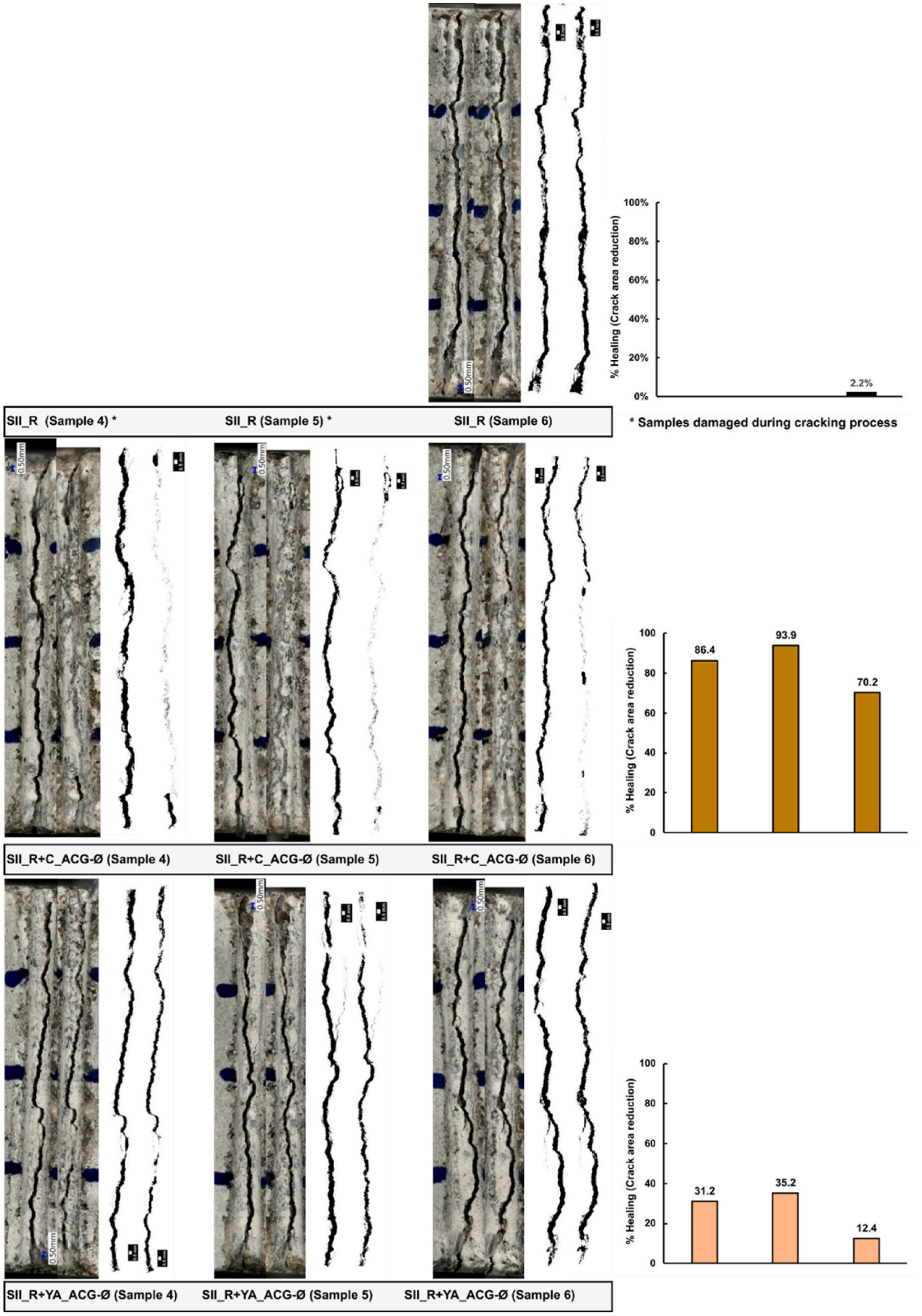
SII_R (Sample 4) *
SII_R (Sample 5) *
SII_R (Sample 6)
% Healing (Crack area reduction)
100%
80%
60%
40%
20%
0%
2.2%
* Samples damaged during cracking process
SII_R+C_ACG-Ø (Sample 4)
SII_R+C_ACG-Ø (Sample 5)
SII_R+C_ACG-Ø (Sample 6)
% Healing (Crack area reduction)
100
80
60
40
20
0
86.4
93.9
70.2
SII_R+YA_ACG-Ø (Sample 4)
SII_R+YA_ACG-Ø (Sample 5)
SII_R+YA_ACG-Ø (Sample 6)
% Healing (Crack area reduction)
100
80
60
40
20
0
31.2
35.2
12.4

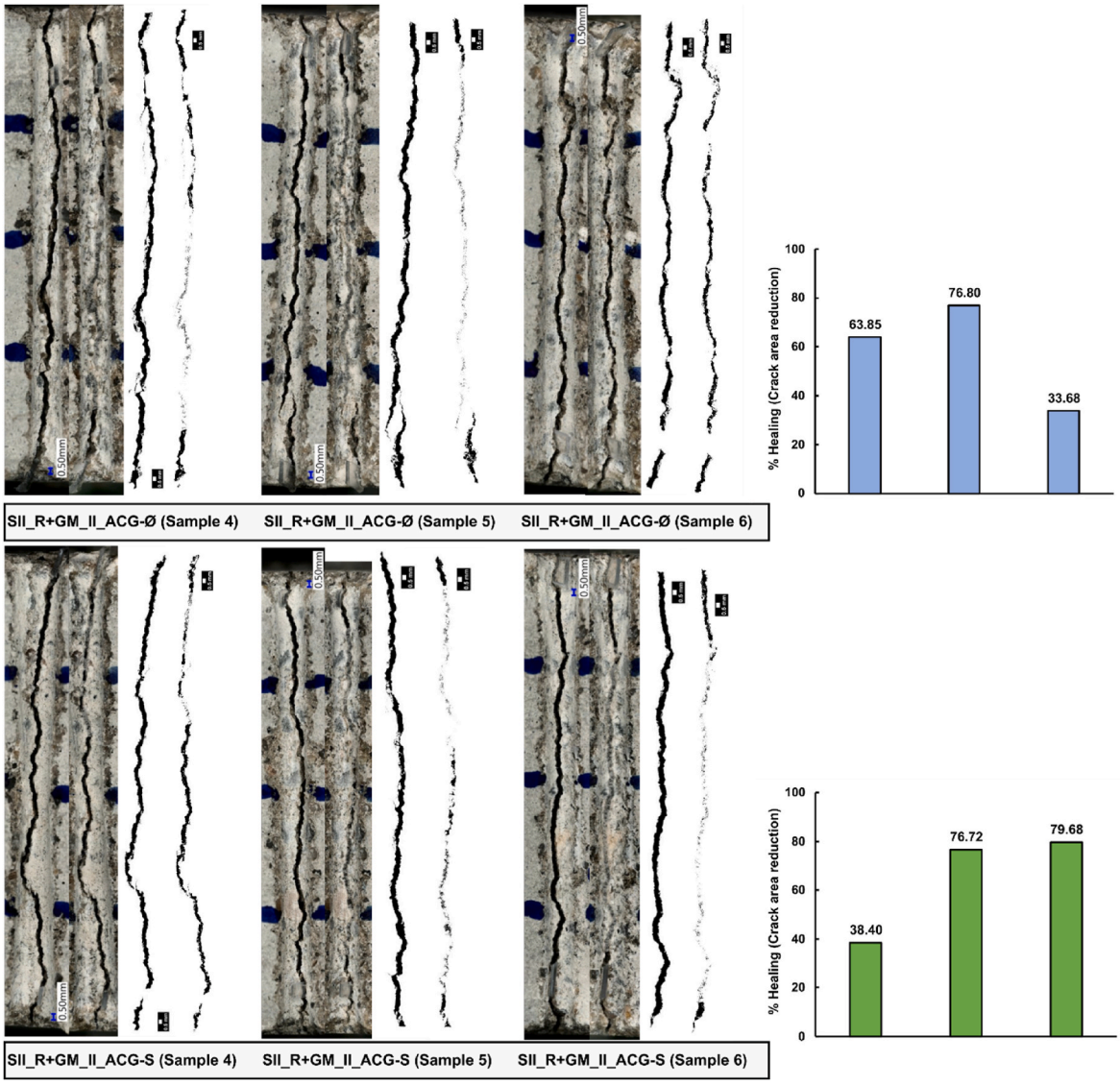
SII_R+GM_II_ACG-Ø (Sample 4)
SII_R+GM_II_ACG-Ø (Sample 5)
SII_R+GM_II_ACG-Ø (Sample 6)
% Healing (Crack area reduction)
63.85
76.80
33.68
SII_R+GM_II_ACG-S (Sample 4)
SII_R+GM_II_ACG-S (Sample 5)
SII_R+GM_II_ACG-S (Sample 6)
% Healing (Crack area reduction)
38.40
76.72
79.68

. (*continued*).

Samples exposed to wastewater (Set II)

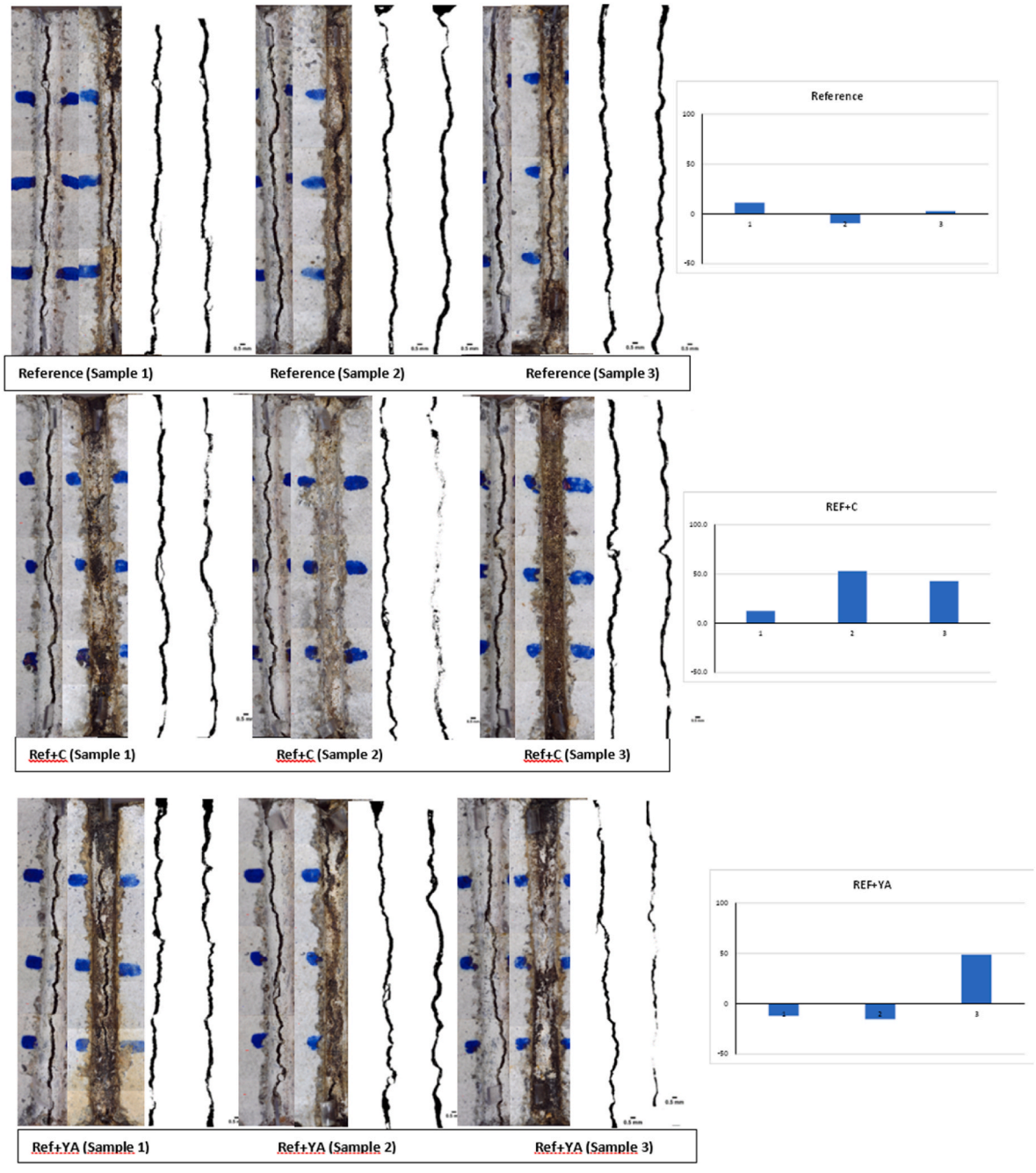

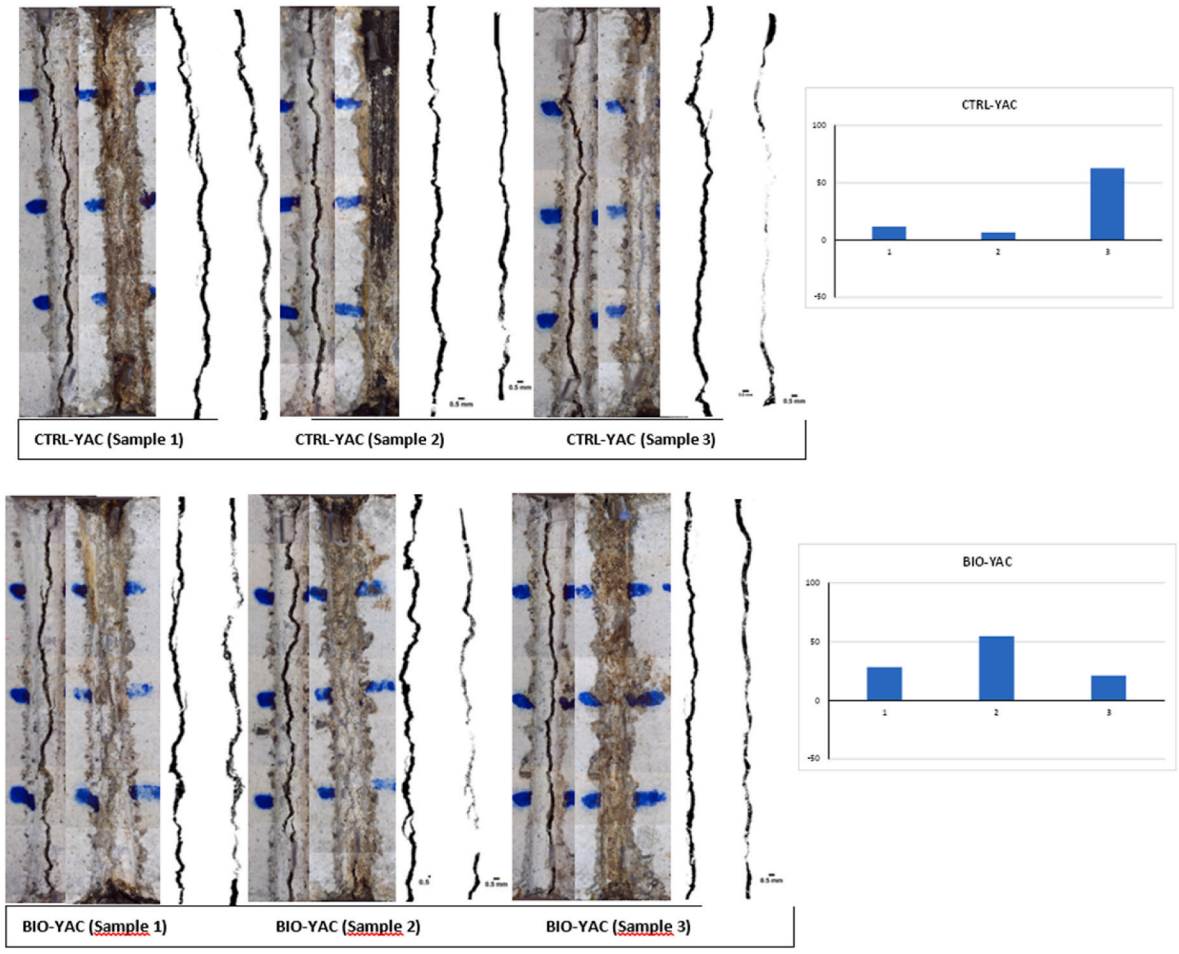

. (*continued*).

Appendix D. Manual assessment of crack opening width

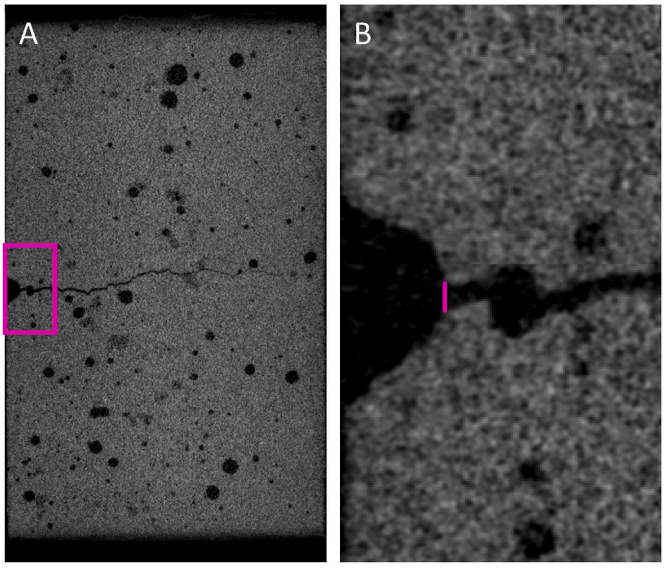

Manual assessment of crack opening width. A) Regions were selected within the brick at spaced intervals. These locations were matched between time points (Day 0 and Day 56). The region of the crack opening (pink box) was assessed and a line drawn within ImageJ to span the shortest distance to connect the walls of the crack at the point of the opening. The distance between these points was measured and compared directly between time points.

References

[1] AJ Englande Jr., P Krenkel, J. Shamas, Wastewater Treatment &Water Reclamation, Ref. Modul. Earth Syst. Environ. Sci. (2015), https://doi.org/10.1016/B978-0-12-409548-9.09508-7. B978-0-12-409548-9.09508-7 Epub 2015 Jul 22. PMCID: PMC7158167.a.

[2] OECD, Financing Water Supply, *Sanitation and Flood Protection*, 2020.

[3] The European Federation of National Associations of Water Services (EurEau), Europe's Water in Figures. An Overview of the European Drinking Water and Waste Water Sectors, 2017, p. 22. Brussels, Belgium.

[4] OSPAR Commission, *Feeder Report* 2021 - *Waste Water*, 2021 (London, UK).

[5] S. Morera, et al., Using a detailed inventory of a large wastewater treatment plant to estimate the relative importance of construction to the overall environmental impacts, Water Res. 122 (2017) 614–623.

[6] S.S. Rashid, Y.-Q. Liu, Assessing environmental impacts of large centralized wastewater treatment plants with combined or separate sewer systems in dry/wet seasons by using LCA, Environ. Sci. Pollut. Control Ser. 27 (13) (2020) 15674–15690.

[7] T.K.L. Nguyen, et al., Contribution of the construction phase to environmental impacts of the wastewater treatment plant, Sci. Total Environ. 743 (2020), 140658.

[8] P. Woyciechowski, et al., Concrete corrosion in a wastewater treatment plant – a comprehensive case study, Construct. Build. Mater. (2021) 303.

[9] ACI Committee 201, ACI 201.2R-08: Guide To Durable Concrete, Farmington Hills, MI, USA, 2008.

[10] M.A. Abd El-Aziz, W.H. Sufe, Effect of sewage wastes on the physico-mechanical properties of cement and reinforced steel, Ain Shams Eng. J. 4 (3) (2013) 387–391.

[11] N. De Belie, et al., A Review of self-healing concrete for damage management of structures, Adv. Mater. Interfac. 5 (17) (2018), 1800074.

[12] V. Cappellesso, et al., A review of the efficiency of self-healing concrete technologies for durable and sustainable concrete under realistic conditions, Int. Mater. Rev. 68 (5) (2023) 556–603.

[13] M. Bagga, et al., Advancements in bacteria based self-healing concrete and the promise of modelling, Construct. Build. Mater. 358 (2022), 129412.

[14] K. Chetty, et al., Self-healing bioconcrete based on non-axenic granules: a potential solution for concrete wastewater infrastructure, J. Water Proc. Eng. 42 (2021), 102139.

[15] I. Justo-Reinoso, et al., Aerobic non-ureolytic bacteria-based self-healing cementitious composites: a comprehensive review, J. Build. Eng. 42 (2021) 1–25, 102834.

[16] W. De Muynck, N. De Belie, W. Verstraete, Microbial carbonate precipitation in construction materials: a review, Ecol. Eng. 36 (2) (2010) 118–136.

[17] S. Farhadi, S. Ziadloo, Self-healing microbial concrete-a review, in: Materials Science Forum, Trans Tech Publ, 2020.

[18] W. Zhang, D. Wang, B. Han, Self-healing concrete-based composites, in: Self-Healing Composite Materials, Elsevier, 2020, pp. 259–284.

[19] N. De Belie, et al., Bacteria-based concrete, in: Eco-efficient Repair and Rehabilitation of Concrete Infrastructures, Elsevier, 2018, pp. 531–567.

[20] B.J. Reeksting, et al., In-depth profiling of calcite precipitation by environmental bacteria reveals fundamental mechanistic differences with relevance to application, Appl. Environ. Microbiol. 86 (7) (2020) 1–16.

[21] W.L. Nicholson, P. Setlow, C.R. Harwood, S.M. Cutting, Molecular Biological Methods for Bacillus, John Willey & Sons, LTD, West Sussex, 1990, pp. 391–451.

[22] L. Tan, et al., Effect of carbonation on bacteria-based self-healing of cementitious composites, Construct. Build. Mater. 257 (2020) 1–13, 119501.

[23] L. Tan, et al., The effects of biomineralization on the localised phase and microstructure evolutions of bacteria-based self-healing cementitious composites, Cement Concr. Compos. (2022), 104421.

[24] Z. Basaran Bundur, M.J. Kirisits, R.D. Ferron, Biomineralized cement-based materials: impact of inoculating vegetative bacterial cells on hydration and strength, Cement Concr. Res. 67 (2015) 237–245.

[25] I. Justo-Reinoso, et al., Air-entraining admixtures as a protection method for bacterial spores in self-healing cementitious composites: healing evaluation of early and later-age cracks, Construct. Build. Mater. 327 (2022), 126877.

[26] L. Ferrara, et al., Experimental characterization of the self-healing capacity of cement based materials and its effects on the material performance: a state of the art report by COST Action SARCOS WG2, Construct. Build. Mater. 167 (2018) 115–142.

[27] M. Roig-Flores, et al., Effect of crystalline admixtures on the self-healing capability of early-age concrete studied by means of permeability and crack closing tests, Construct. Build. Mater. 114 (2016) 447–457.

[28] C.A. Schneider, W.S. Rasband, K.W. Eliceiri, NIH Image to ImageJ: 25 years of image analysis, Nat. Methods 9 (7) (2012) 671–675.

[29] M. Luo, C.-x. Qian, R.-y. Li, Factors affecting crack repairing capacity of bacteria-based self-healing concrete, Construct. Build. Mater. 87 (2015) 1–7.

[30] M. Luo, et al., Crack self-healing of cement mortar containing ureolytic bacteria immobilized in artificial functional carrier under different exposure environments, Buildings 12 (9) (2022) 1348.

[31] M. Luo, et al., Self-healing of early-age cracks in cement mortars with artificial functional aggregates, Construct. Build. Mater. 272 (2021), 121846.

[32] I. Justo-Reinoso, et al., Evaluation of cyclic healing potential of bacteria-based self-healing cementitious composites, Sustainability 14 (11) (2022) 1–15.

[33] RILEM, RILEM Test Method 11.4: Measurement Of Water Absorption under Low Pressure, RILEM, Paris, France, 1987.

[34] T. Van Mullem, et al., Novel active crack width control technique to reduce the variation on water permeability results for self-healing concrete, Construct. Build. Mater. 203 (2019) 541–551.

[35] J. Schindelin, et al., Fiji: an open-source platform for biological-image analysis, Nat. Methods 9 (7) (2012) 676–682.

[36] B.D. Ondov, N.H. Bergman, A.M. Phillippy, Krona: interactive metagenomic visualization in a web browser, in: K.E. Nelson (Ed.), Encyclopedia of Metagenomics, Springer New York, New York, NY, 2013, pp. 1–8.

[37] S.L. Williams, M.J. Kirisits, R.D. Ferron, Optimization of growth medium for Sporosarcina pasteurii in bio-based cement pastes to mitigate delay in hydration kinetics, J. Ind. Microbiol. Biotechnol. 43 (4) (2016) 567–575.

[38] M. Vandervoort, Impact Of Bioagents on the Cementitious Matrix, Ghent University, 2019.

[39] P. Risdanareni, et al., Suitable yeast extract concentration for the production of self-healing mortar with expanded clay as bacterial carrier, Mater. Construcción 72 (348) (2022) e296-e296.

[40] L. Black, et al., Structural features of C–S–H (I) and its carbonation in air—a Raman spectroscopic study. Part II: carbonated phases, J. Am. Ceram. Soc. 90 (3) (2007) 908–917.

[41] J. Sun, et al., A Raman spectroscopic comparison of calcite and dolomite, Spectrochim. Acta Mol. Biomol. Spectrosc. 117 (2014) 158–162.

[42] J.L. Zhang, et al., Screening of bacteria for self-healing of concrete cracks and optimization of the microbial calcium precipitation process, Appl. Microbiol. Biotechnol. 100 (15) (2016) 6661–6670.

[43] M.J. Al-Kheetan, et al., Development of low absorption and high-resistant sodium acetate concrete for severe environmental conditions, Construct. Build. Mater. 230 (2020), 117057.

[44] M.J. Al-Kheetan, et al., Microstructural, mechanical and physical assessment of portland cement concrete pavement modified by sodium acetate under various curing conditions, Infrastructure 6 (8) (2021) 113.

[45] M.J. Al-Kheetan, M.M. Rahman, Integration of anhydrous sodium acetate (ASAc) into concrete pavement for protection against harmful impact of deicing salt, JOM 71 (12) (2019) 4899–4909.

[46] W. Zhang, et al., Self-healing concrete composites for resilient infrastructures: a review, Compos. B Eng. (2020), 107892.

[47] I. Uad, et al., Precipitation of carbonates crystals by bacteria isolated from a submerged fixed-film bioreactor used for the treatment of urban wastewater, Int. J. Environ. Res. 8 (2014) 435–446.

[48] D. Arias, L. Cisternas, M. Rivas, Biomineralization mediated by ureolytic bacteria applied to water treatment: a review, Crystals 7 (11) (2017).

[49] F. Hammes, et al., A novel approach to calcium removal from calcium-rich industrial wastewater, Water Res. 37 (3) (2003) 699–704.

[50] S.B. Mahat, et al., Phenomena of Bacillus sphaericus LMG 22257 activity and its influence on properties of portland cement mortar exposed to different curing media, Separations 10 (1) (2023) 19.

[51] F.B. Silva, et al., Industrial application of biological self-healing concrete: challenges and economical feasibility, J. Commerc. Biotechnol. 21 (1) (2015) 31–38.

[52] W. Khaliq, M.B. Ehsan, Crack healing in concrete using various bio influenced self-healing techniques, Construct. Build. Mater. 102 (2016) 349–357.

[53] E. Tziviloglou, et al., Bacteria-based self-healing concrete to increase liquid tightness of cracks, Construct. Build. Mater. 122 (2016) 118–125.

[54] K. Vijay, M. Murmu, Self-repairing of concrete cracks by using bacteria and basalt fiber, SN Appl. Sci. 1 (11) (2019).

[55] Y.C. Ersan, et al., Self-protected nitrate reducing culture for intrinsic repair of concrete cracks, Front. Microbiol. 6 (2015) 1228.

[56] H. Huang, G. Ye, D. Damidot, Characterization and quantification of self-healing behaviors of microcracks due to further hydration in cement paste, Cement Concr. Res. 52 (2013) 71–81.

[57] J. Wang, et al., X-ray computed tomography proof of bacterial-based self-healing in concrete, Cement Concr. Compos. 53 (2014) 289–304.